Internet of Things for Environmental Sustainability and Climate Change

Chapter · January 2020

DOI: 10.1007/978-3-030-35291-2_2

1 author:

Abdul Salam
Purdue University West Lafayette
87 PUBLICATIONS **3,362** CITATIONS

https://doi.org/10.1007/978-3-030-35291-2_2

Chapter 2
Internet of Things for Environmental Sustainability and Climate Change

Abstract Our world is vulnerable to climate change risks such as glacier retreat, rising temperatures, more variable and intense weather events (e.g., floods, droughts, and frosts), deteriorating mountain ecosystems, soil degradation, and increasing water scarcity. However, there are big gaps in our understanding of changes in regional climate and how these changes will impact human and natural systems, making it difficult to anticipate, plan, and adapt to the coming changes. The IoT paradigm in this area can enhance our understanding of regional climate by using technology solutions, while providing the dynamic climate elements based on integrated environmental sensing and communications that is necessary to support climate change impacts assessments in each of the related areas (e.g., environmental quality and monitoring, sustainable energy, agricultural systems, cultural preservation, and sustainable mining). In the IoT in Environmental Sustainability and Climate Change chapter, a framework for informed creation, interpretation and use of climate change projections and for continued innovations in climate and environmental science driven by key societal and economic stakeholders is presented. In addition, the IoT cyberinfrastructure to support the development of continued innovations in climate and environmental science is discussed.

2.1 Introduction

The global climate is changing rapidly mainly because of the human activities over the period of last five decades [80, 137]. This change is project to continue in the foreseeable future depending on the heat-trapping gas emissions in the environment and sensitivity of the climate of the Earth on these emissions [108]. From 1895 to 2020, an increase of 1.3–1.9 °F in average temperature has been observed in the USA with substantial increase after the year 1970 [7, 25, 110]. The change in global annual mean surface-air temperatures (ocean and land combined) is shown in Fig. 2.1. An increase of 8 in. has been observed in global sea levels since 1880 with a projected increase of up to 4 ft by the end of this century. The ice covered areas (surface extent) in sea, land, and lakes are decreasing with increase in temperature [63, 116]. The warmest month records are being

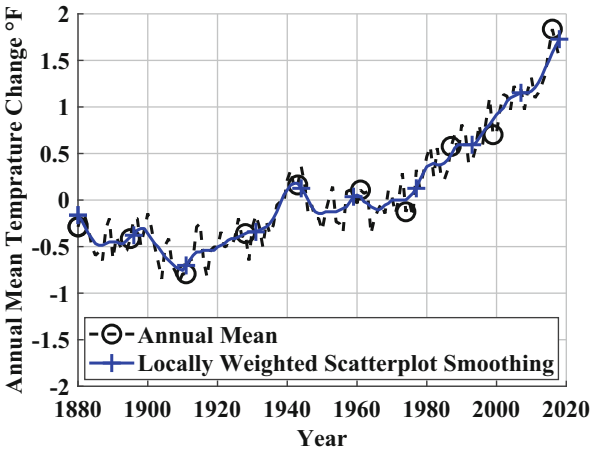

Fig. 2.1 The change in global annual mean surface-air temperatures (ocean and land combined) based on NASA/GISS/GISTEMP data

broken consistently and human caused global warming combined with natural changes in climate is making too difficult to accurately predict climate variations [8, 79, 117, 119, 124]. Accordingly, due to the interdependence of the growing season on the frost-free period, the length of growing season has been increased and will continue to increase [4, 30, 38, 62, 68, 74, 142, 157, 158, 173]. Moreover, the average precipitation has increased with corresponding increase in intensity of the extreme downpours and precipitation [7, 94, 128, 139, 151]. Furthermore, more variations are being observed in extreme weather occurrence patterns (e.g., the frequency of the cold waves have decreased but its intensity has increased) [9, 32, 44, 55, 83, 120, 146]. Similarly, the same patterns are being observed for droughts and flooding, where droughts intensity has increased [49, 82, 121]. Since 1980, the hurricanes have become more frequent and intense spanning over longer duration which is also related to the heavy downpours and intense storms [20, 43, 106]. The frequency and intensity of the winter storms, damaging winds, thunderstorm, and tornadoes are also the subject of climate change investigation [17, 65, 112, 155]. The ocean acidification (the decrease in the pH levels of the oceans) is increasing due to the one-fourth absorption of the atmospheric carbon dioxide emission in oceans which is impacting marine echo system [33]. The change in annual mean surface-air temperatures in USA is shown in Fig. 2.2.

The IoT is being envisioned as an effective tool to combat the climate change [81]. Through its sensing and monitoring capabilities, it provides insights into root cause of climate change by sensing the amount of CO_2 and different greenhouse gases in our atmosphere [150]. The emissions of greenhouse gases from burning of fossil fuels can be sensed in real time. Accordingly, the carbon sequestration processes and rates can be monitored to increase the storage of carbon captured in forests which helps to offset emissions. Furthermore, the novel atmospheric "things" and technology can be developed to permanently reduce the atmospheric CO_2 with integration into the climate IoT.

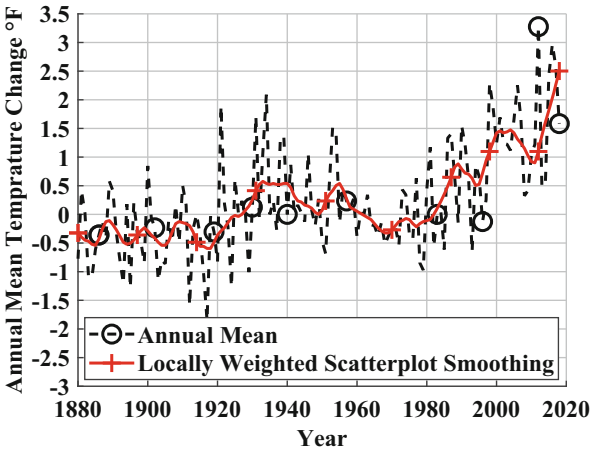

Fig. 2.2 The change in annual mean surface-air temperatures in USA based on NASA/GISS/GISTEMP data

The climate IoT is also useful in climate change anticipation and adaption preparation. Its sensing and communication technologies coupled with prediction systems and models clear uncertainty and provide useful insights into the exact nature of the climate changes. The IoT enabled climate decision making tools can predict predicting how the climate will change and how the ecosystem is likely to respond to the climate change and other factors affecting it. The IoT technology has enabled empirical investigations on impacts of elevated greenhouse gases [126]. It also supports simulations of ecosystem's response in different climatic conditions (both current and future). With this new knowledge the environmental and atmospheric management practices are tailored and accordingly novel management techniques can be developed. By utilizing the contemporary scientific and technological advancements, the climate IoT has the potential to meet immediate and long-term goals and applications needs. This architecture provides better understanding and insights into the global ecosystems and supports informed decision making. This enhanced understanding of the Earth system from universal to regional scales has the potential to enhance our ability to assess water resources, predict weather patterns, forecasts climate, and increased understanding of ecosystem health. The impact of these factors on our community determines the need of development of applications utilitarian to the society.

2.2 Climate Change IoT Things for Environmental Sustainability

The worldwide environment consists of the atmosphere, ecosystems, air quality, hydrosphere, lithosphere, atmosphere chemistry, chromosphere, biosphere, land and ocean bio-geochemical processes [77]. The following climate change elements

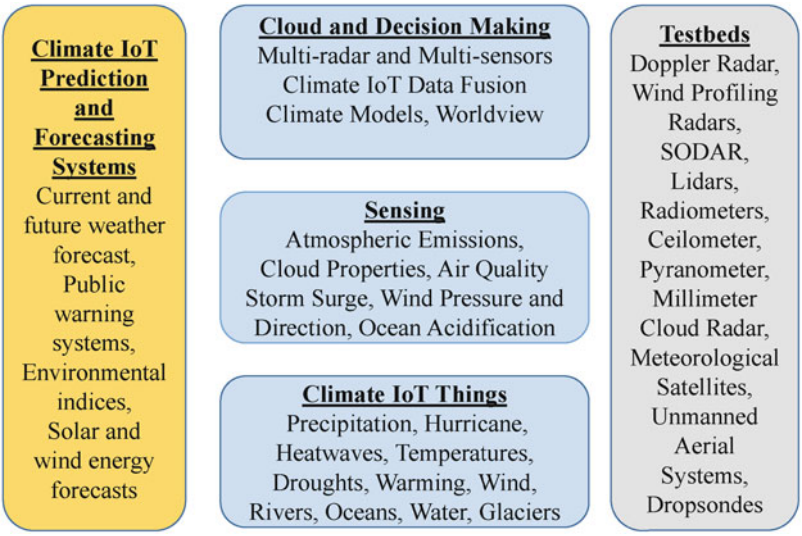

Fig. 2.3 The architecture of environmental sustainability and climate change IoT

outline main contextual components related to functionalities of the IoT in environmental sustainability and climate change (Fig. 2.3):

- Severe precipitation, hurricane, and heatwaves events
- Storm surge, shoreside and in-land flooding, and increase in sea levels
- Ocean acidification and alteration of marine ecosystems
- Decline in water availability and elevated water competition aggravated by increase in population and land-use practices
- Surging carbon dioxide levels
- Rising temperatures, droughts, and warming caused by wildfires
- Enhanced demand of water for energy and water
- Variation in timing of streamflow caused by snow melt
- Shrinking glaciers and permafrost thawing
- Water scarcity and reducing supplies of fresh water

2.3 Climate IoT as the Sustainability Enabler Framework

2.3.1 Holistic System

The integration of sensors, communication technologies, reporting, prediction, and forecasting and surface meteorological systems in the environmental sustainability and climate change IoT paradigm has many potential benefits [159]. Novel

visualization and decision-support tools for changes in ocean temperature, coastal inundation, and sea-level at decision-relevant scale can be developed for real-time analysis using multi-radar and multi-sensors IoT elements. These systems will serve as indicators of climate impacts on ocean and coastal resources and other sectors which will aid in enhanced weather forecasting using adaptive atmospheric sensing and sampling and radar technology with resolution of 10,000 m for deterministic forecast and 20,000 m for ensemble forecast.

2.3.2 Novel Sensing Methods

The data from new sensors and robotic floats for biogeochemical, biooptical, and pH measurements can be fused in the cloud for real-time analysis [104]. The multi-dimensional atmospheric analysis prototypes can be integrated into the system with data assimilated from wide area meteorological zones for providing robust warnings using real-time radar sampling techniques. The environmental sustainability and climate change IoT paradigm can help prototyping the weather and fire behavior modeling system for local firefighting applications. The climate IoT paradigm brings improvements in accurate understanding and better planning by enabling climate forecasts at multi-time-scales, projections of future climate trends and change for support policy decisions. It enables integration of following sensing and monitoring systems.

2.3.3 Solar Radiation and Soil Moisture Data

In environmental sustainability and climate change IoT paradigm, the solar radiation and soil moisture data can be linked for improved insights into the wind, water content, and temperature profiles [37]. The aerial sensing systems composed of different types of sensors (e.g., LiDAR, Doppler radar, spectrometer, dropsondes [131], and radiometer) also provide diverse insights [91, 156]. These observations are useful to fill gaps in measurements of different parameters of water cycle including water vapor transport, precipitation, snow, river flow, sea-ice, waves, water level, and surface energy budget terms including evapotranspiration and aerosols. Moreover, the impact of natural changes such as solar and volcanic activities, varying aerosols and greenhouse gases radiative forcing can be observed at large scale.

- Tropical and extra tropical oceans and cyclones, ocean basin, and sea levels
- Storm surges, droughts, heat waves, and wildfires
- Land-based ice sheets and hydrologic cycle
- Simulations of ocean, atmosphere, and land-surface processes
- Surface albedo, water vapor, clouds, and geomagnetic conditions

- Temperature, precipitation, extreme events, and pollution
- Air quality modeling, wildfires, and dust storms

2.3.4 Forecasting Models

For understanding and predicting the impacts of climate variabilities, extreme and precipitate climate changes, there is a strong need of full range of tools for environmental prediction and projection forecasts on different spatial and temporal scales [11, 123]. The climate IoT paradigm is also useful to ascertain the effects of the slowly changing Arctic Oscillation (AO) weather patterns through simulations [8]. New insights can be gained about the impact of ocean-atmosphere link on weather forecast through interconnection if these currently disjoint systems [40]. Similarly, it enables hurricane inner nest for global forecasting system. The advantages of multi-model, stochastic-, and multi-physics ensemble generation can be realized with novel methods of uncertainty condition representation [2]. Moreover, with the data obtained from the sensing and monitoring systems, the advanced statistical models can be developed for reliability improvement (e.g., tropical storm and extra-tropical storm inundation model) [59, 111, 118, 143]. It also enables development of new disciplines such as storm behavior climatologies by providing access to data collected over span of multiple decades. Furthermore, prototypes of high resolution climate models and prediction systems can be developed including novel downscaling methods for climate systems across different temporal/spatial scales [12, 42, 48, 49, 51, 138]. The data assimilation process in ionosphere and thermo-sphere in forecast models can provide better insights. A global climate grid scale model is shown in Fig. 2.4. Other important models are listed below:

- Route inundation storm surge
- Storm scale
- Geospace model in local geomagnetic storm
- Radiation environment at aviation and orbital altitudes
- Assimilative models
- Ionosphere plasmasphere
- Wind energy
- Coupled human and natural systems

2.3.5 Emissions Monitoring

The black carbon, methane, and nitrous oxide emissions can be quantified through climate IoT sensing techniques with high certainty [10, 45, 58, 75, 90, 92, 93, 101, 149, 154, 167, 170]. Accordingly it impact on the environment and clouds can be

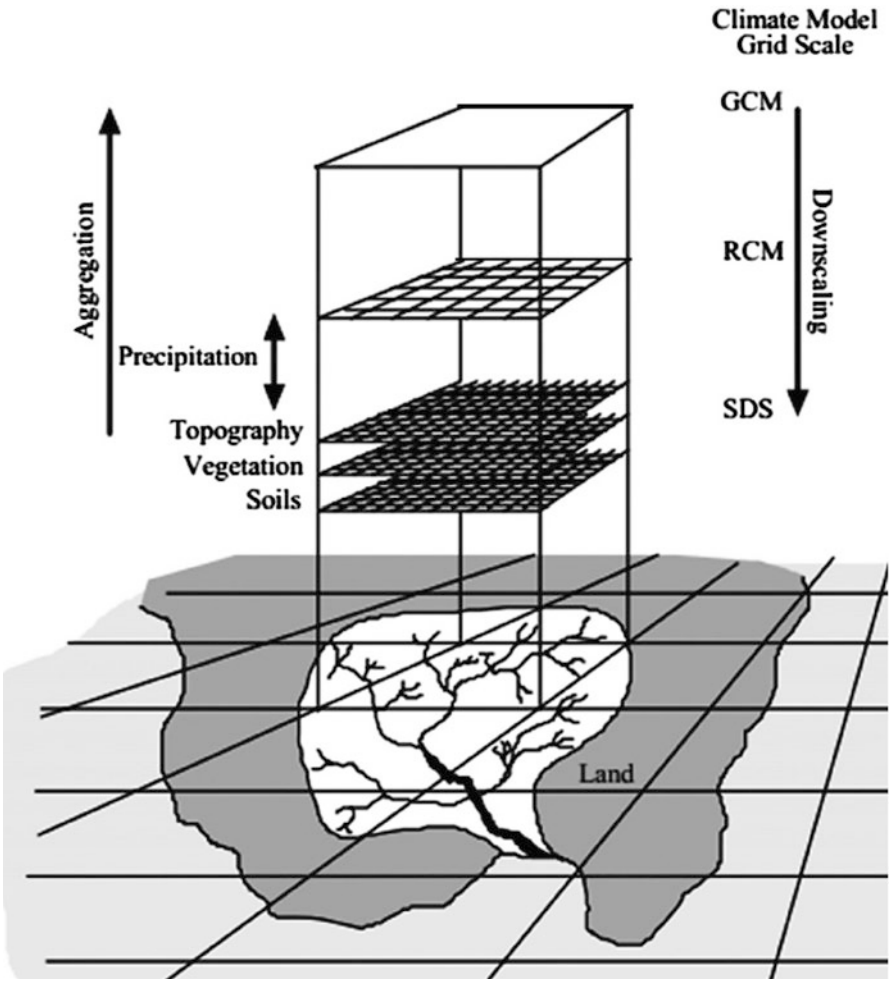

Fig. 2.4 The global climate grid scale model [136]

assessed by developing reliable flux estimates. The impact of four replacement compounds on extremely high ozone layer, surface air quality, and climate can be evaluated for solvents, refrigerants, and other blow agents [13, 16]. It also enables air chemistry assessment of effects of urban, gas, and oil development emissions on urban air quality [144]. Moreover accurate models can be developed to quantify climate sink and forcing for the following:

- Atmospheric aerosols
- Greenhouse gases
- Aerosol interactions
- Stratospheric chemistry

2.4 Climate Communication Technologies and Systems

With the advancement in systems development, many novel atmospheric monitoring and mapping, and communications technologies have been developed. These are discussed in the following section.

2.4.1 Doppler Radar

Data about the velocity remote objects can be obtained using a special type of radar that measures the Doppler effects [23, 95]. A microwave EM signal is transmitted from the radar towards the desired target that is in motion [22, 41]. The frequency of returned signal (bounced from the object) is analyzed to get accurate measurement of target speed.

The Doppler effect can be produced using four different methods:

- Coherent pulsed (CP)
- Pulse-Doppler
- Continuous wave (CW)
- Frequency modulation (FM)

The narrow-band filters are employed in Doppler radars to cancel interference from low speed and immobile objects (e.g., birds, clouds, insects, and wind) (Fig. 2.5).

2.4.2 Wind Profiling Radars

Wind profiling radar (also called wind profiler) [61, 98] is a type of Doppler radar that functions in the VHF frequency band from 30 to 300 MHz and UHF frequency band 300–1000 MHz frequency bands. It operates by directing the beam energy to the normal offset by few degrees. The wind profiling radar differs from the scanning Doppler in their processing and production of Doppler [97]. In the profiler, hundreds of low intensity pulses are transmitted to create Doppler velocity spectrum with a 30 s of dwell time. Whereas, in Doppler scanning radar resolved volume moments are produced by a limited number of pulses are transmitted with dwell time of few milliseconds.

2.4.2.1 Types of Wind Profiling Radars

Different types of wind profiling radars are explained below [147]:

- 404 MHz NOAA profiler network (NPN) Profiler is used for the deepest atmospheric coverage. It uses coaxial-collinear phased array antenna with antenna

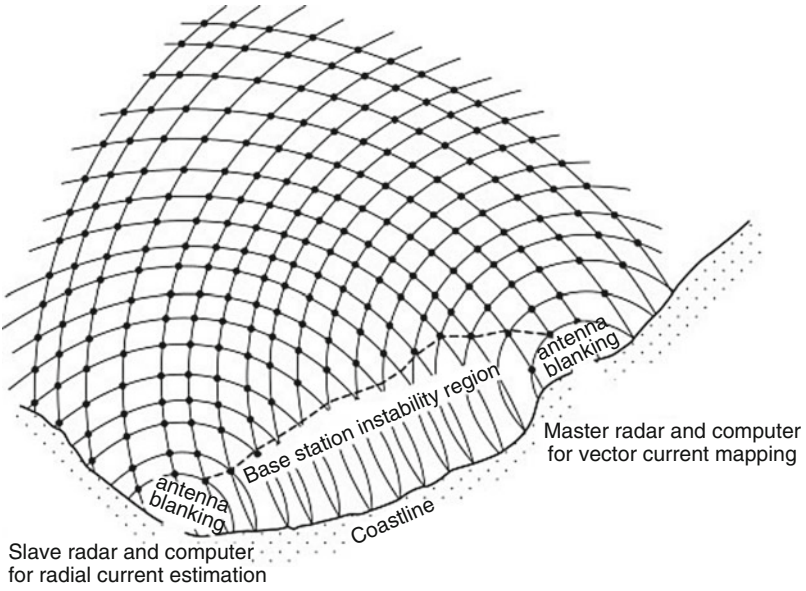

Fig. 2.5 Conceptual rendition of the spatial coverage of dual-site HF/VHF Doppler radar systems using two wide-beam transmit antennas. The dots represent the locations on the sea surface from which radial water-current vectors are derived using echoes received at both the radars [78]

diameter of 13 m and beamwidth of 4°. It can cover a height of up to 16,000 m with vertical resolution of 900 m. With peak transmit power of 6000 W, it can attain temporal resolution of 60 min. Due to its sophisticated hardware, it is considered expensive to fabricate and operate.

- 915-MHz boundary layer profiler is easy to build and operate yet it has limited height measurement capability beyond the boundary layer. It uses flat rectangular microstrip patch antenna with antenna diameter of 2 m and beamwidth of 10°. It can cover a height of up to 4000 m only with vertical resolution of 106 m. With peak transmit power of 500 W, it can attain temporal resolution of 60 min.
- 915-MHz quarter scale profilers are also easy to build and its height measurement capability is better than the boundary layer profiler. It uses coaxial-collinear phased array antenna with antenna diameter of 6 m and beamwidth of 10°. It can cover a height of up to 8000 m only with vertical resolution of 212 m. With peak transmit power of 2000 W, it can attain temporal resolution of 60 min.

The wind profiling radars can operate in two different modes: the Doppler beam swinging (DBS) and radio-acoustic sounding system (RASS) modes. Both modes are not supported simultaneously.

- In Doppler beam swinging (DBS) the beam is steered in three to five different radial directions for Doppler spectra measurements. Accordingly, the motion

of the horizontal winds radial component is measured for each direction to determine the horizontal wind profile. The longer time duration high mode pulse and shorter duration low mode pulses are employed for low and high height resolution, respectively.

- In Radio-acoustic sounding system (RASS) mode acoustics wave and radio waves are employed simultaneously to determine. The velocity of sound wave is analyzed as function of height to determine vertical air motion and temperature.

2.4.2.2 Sonic Detection and Ranging (SODAR)

The sonic detection and ranging (SODAR) is a type of wind profiling radar that is used for meteorological purposes [26, 97, 99]. The sound waves are impacted by turbulence when propagating in the atmosphere. SODAR measures that scattering process to determine the above-ground wind speed at different heights. It is also used to analyze the thermodynamic structure of the low atmospheric region. It is based on the Doppler effect mechanism of the frequency change of sound waves relative to the moving target. It operates in the 4.5 KHz sound wave spectrum. Three different acoustic beams are transmitted. A vertical beam which goes straight upwards and two beams are emitted at 17° normal to the Earth. The reflected signal is received and fast Fourier transform (FFT) operation is performed for frequency domain analysis. Accordingly, the Doppler-shifted frequency is used to determine the wind speed. It works for the height range of up to 200 m.

In bi-static SODARs the sender and receiver can be located at a distance (usually up to 10 m) instead of being housed in the same unit. In conventional setting, SODARs are only able to get measurements from a fixed height. With electronically scanned array of acoustics microphones, the receiver can get multiple views from different heights with accurate measurements of velocity variations in turbulence.

2.4.2.3 Wind Profiling LiDARs

LiDAR (light detection and ranging) is used to illuminate the target by using laser light and sensing the reflectance by using light sensors [114, 123]. A 3-D results can be produced by using the delay in laser arrival time and wavelengths. A wind profiling also works on the Doppler effects principal where the back-scattering of light particles from the atmosphere is used to measure the wind turbulence and speed at different heights. The performance can be further improved by using laser beam steering mechanism where interference form the undesired components can be reduced or totally eliminated to produce high quality results.

2.4.3 Microwave Radiometers

At larger wavelengths in the spectrum, the microwave measurements of the electromagnetic (EM) radiation are used for wavelengths between 1 mm and 1 m [15]. Microwave measurements are classified into the longwave and shortwave measurements. These are explained in the following:

2.4.3.1 Longwave Measurements

The longwave measurements are done using wavelengths that are longer than approximately 4.0 μm. These are further classified into three types:

Longwave Broadband The longwave broadband measurements are used for direct radiant energy diffusing in vertical upward and downward direction within the broadband and infrared wavelengths [51].

Longwave Spectral The longwave spectral measurements are employed for radiant energy resolving in spectrum at infrared wavelengths.

Longwave Narrowband It includes radiant energy measurements in the narrowband infrared wavelengths.

2.4.3.2 Shortwave Measurements

The shortwave measurements are done using wavelengths that are less than 4.0 μm. These are further classified into three types:

Shortwave Broadband The shortwave broadband microwave is used to measure the intensity of the radiant flux in the visible spectrum and infrared-approaching spectrum chunks of the shortwave broad-wavelength bands.

Shortwave Narrowband The shortwave narrowband is employed to measure the intensity of the radiant flux in the visible and infrared-approaching spectrum chunks in shortwave narrow-wavelength bands.

Shortwave Spectral The shortwave spectral measurements of radiant energy flux intensity are done at spectrum resolving visible and infrared-approaching wavelengths.

Radiometers are receivers of the frail EM energy which is transmitted from the surface of the earth, whereas the radars transmit their own EM pulses to the surface [15, 96]. The radiometric measurements are done using different methods such as active radar, active LiDAR, passive broadband radiometers, and passive sensors [127]. The measurements are important source atmospheric data which is obtained by measuring the decay of the energy of the electromagnetic waves when traveling through the atmosphere.

2.4.4 Ceilometer

A ceilometer is an aerosol concentration measurement device that operates on the light sources such by using laser to obtain the cloud heights and base [27]. It is considered as a type of the LiDAR with much less range. There are two different types of the ceilometers.

2.4.4.1 Optical-Drum Ceilometer

An optical-drum ceilometer consists of a detector, recorder, and moving projector and works on the triangulation technique to get the height of the cloud based light spot projection.

2.4.4.2 Laser Ceilometer

A laser ceilometer carries both the laser transmitter and receiver in the same unit and has the capability to transmit very short pulses of few nanoseconds duration to the atmosphere. These work on the same principles as the LiDAR and can be used to map atmospheric volcanic ashes and clouds.

2.4.5 Microbarographs

The microbarograph, also named as barograph, is used to measure pressure of the atmosphere in millibars with reference to sea levels. A graph paper, wrapped around the moving cylindrical bar, is used for recording the continuous pressure [64].

2.4.6 Pyranometer

A pyranometer is a device to determine flux density of solar radiation in hemisphere. It measures solar irradiance by surfaces of planar shapes [107]. Pyranometer is a special type of actinometer with wavelength range of 0.285 to 2.8 μm. It is used for measuring solar irradiance on a planar surface and it is designed to measure the solar radiation flux density from the hemisphere above within a wavelength range of 300–3000 nm. The sun emits solar radiation, which can be harvested for heat and electric energy uses. Many environmental indexes are produced from the data acquired from the pyranometer such as temperature, humidity, sun, and wind (THSW) and ET. Aerosol characteristics (e.g., scattering, phase, refraction index) can be produced through photometer sky radiance measurements inversion. Sun

photometer instrument is used to measure radiance at four frequencies in various scanning scenarios. The aerosol optical depth (AOD) is also measured using this instrument.

2.4.7 Millimeter Cloud Radar

The millimeter cloud radar (MMCR) works on the measurement of vertical speed of the particles also called the Doppler velocity [3, 28]. When clouds are above the radar, the MMCR measures its vertical profile by using the reflectivity which is a measure of the intensity of the returning signal. Accordingly, the size of the cloud particle is determined by using colors. A rising particle is indicated by a warm color and fall particles are specified by cool colors. Similarly, the width of spectrum shows the diversity of the cloud particles (the typical particle size is approximately 0.2 μm.)

2.4.8 Sonic Anemometers

An anemometer is an instrument commonly found on meteorological stations. It is used for rapid 3-dimensional wind speed measurements with higher accuracy. It is also used for turbulence measurements [66]. It supports sub-meter (0.01 m/s resolution) in 6000 cm range with rates of 0.1 KHz which is helpful for detailed turbulence analysis. Sonic anemometers operate by measuring the time taken for a pulse of sound to travel between a pair of acoustic radios (both radios are equipped with transmission and reception facility, which is alternated for bi-directional measurements). Since, the velocity of the sound wave is affected by many factors (e.g., fog, dust, temperature, and pressure), accurate measurement requires sensitive anemometer equipment. Moreover, the heavy downpour also affects the measurements and leads to variations in pulse travel time. Similar type of errors is also observed in icy conditions requiring anti-ice warming equipment to be integrated with the equipment. To reduce the effects of the distortions caused by the air flow, calibrations are performed in wind tunnels to correct direction related errors. The wind angle and direction can be measured by employing more than two radios. It supports operation in 0.02, 0.05, and 0.1 kHz frequency bands.

2.4.9 Environmental and Meteorological Satellites for Remote Sensing

Meteorological satellite plays a vital role in climate change and variability analysis. These are used to obtain the meteorological, oceanographic, and terrestrial data

of the Earth [6, 18, 19, 35, 36, 130, 160]. The meteorological and environmental satellites are used for different types of EM waves measurements that are either emitted or reflected form the Earth such ocean and land surface and from the atmosphere [18, 39, 67, 71]. These satellites have the capability to measure the wide range of EM spectrum including the visible light spectrum, radiations in microwave and infrared bands [61, 76]. These are explained in the following sections.

2.4.9.1 Geostationary Satellites

The geostationary satellites functions in orbits and these spin in the direction of Earth rotation [164]. Therefore, with reference to the surface of the Earth, a static position is maintained over the Earth at very high altitude (23,922 miles). Due to this factor, these satellites have the capability to observe the same region of the Earth and are frequently used in weather applications such as cloud properties sensing. However, in comparison to the low altitude satellites, high resolution analysis cannot be supported. These satellites provide consistent data flow to ground stations about the planet after every half hour. Two main instruments on the GOES satellite are an imaging and sounding system. The imaging instrument supports are capable of taking measurements at four different frequencies in visible, water vapor infrared and thermal infrared spectrum for cloud water, and surface temperature monitoring. The Geostationary Operational Environmental Satellite (GOES) East and West are the two examples of the geostationary satellites:

- The Geostationary Operational Environmental Satellite East is also known as GOES-12. It is located 75° west longitude over the equator at 7. It is used to cover the American continent.
- The Geostationary Operational Environmental Satellite West satellite, positioned over 135° west longitude, this is also called GOES-10. The eastern pacific region is covered by these satellites. Similar satellites are also being operated to cover the provide coverage at global scale
- The Geosynchronous Meteorological Satellite (GMS) is also known as GMS-5. It is used to cover the western pacific region. It is located over the equator at 140° east longitude. With the exception equipment of sounding hardware, all equipment found on the GOES-West and GOES-East satellites are also present on the GMS with same imaging capabilities.

2.4.9.2 Polar-Orbiting Satellites

The polar orbiting satellites generally are in comparatively low altitudes circular orbits in comparison to the geostationary satellites. The typical height is approximately 435–500 miles and it takes 1.6 h to complete the orbit. Moreover, as compared to geostationary satellites, their position is not fixed rather these

continuously change their position with relative to the surface of the Earth. These can provide high resolution imaging but complete coverage of the Earth takes many days by using multiple satellites.

Examples of the polar-orbiting satellites are given below:

- The Defense Meteorological Satellite Program (DMSP). These are used to provide meteorological coverage on diurnal basis about the oceanographic, meteorological, and terrestrial properties of the planet. DMSP satellites orbit at an altitude of approximately 830 km, collecting images across a 3000-km swath under both daytime and nighttime conditions. Each satellite views any point on the Earth twice a day and completes an orbit in about 101 min. Complete global coverage is provided every 6 h. The measurement instrument on DMSP satellites includes the Special Sensor Microwave Imager (SSM/I) [47, 69, 133, 163] for geophysical parameters, the SSM/T, and the SSM/T2 (atmospheric sounding instruments for microwave temperatures at different heights). These are used to gather data at four different frequencies using two polarization settings. The geophysical data provided by SSM/I consists of wind speed and temperature at ocean surface, land and water precipitation, and atmospheric water vapor.
- The NOAA Polar-orbiting Operational Environmental Satellites (POES) provide daily coverage
- Landsat satellites. Supports higher resolution and multi-spectral imaging
- French SPOT satellites. No daily coverage capability

2.4.9.3 More Meteorological Satellites

More weather imaging and atmospheric monitoring satellites are also used globally such as European Community operates Meteosat, China operates the Feng-Yun, Russia operates GOMS, and INSAT satellite is operated by India. Features of these satellites are explained in the following:

- Meteosat is a type of geostationary satellite. It is operated by the European Organization for the Exploitation of Meteorological Satellites (EUMETSAT). Meteosat is used to obtain data using visible light, thermal infrared, and water vapor infrared wavelengths.
- Feng-Yun is operated by also a geostationary meteorological satellite. It is located at 105° east longitude. It is equipped with visible wavelength sensor system that senses radiation in one visible frequency and two infrared frequencies. This equipment has the capability of producing visible imaging of the Earth on a particular day.
- GOMS has the infrared equipment and is also Elektro and GOMS-1. It works on the geosynchronous weather imaging technology.
- The Indian INSAT satellite is located above the equator at approximately 90° east longitude. It is used to obtain images of Central Asia and Indian Ocean.

2.4.10 GPS Signals for Remote Sensing

A remote sensing tool has been proposed which uses signals from GPS satellite systems for sensing applications where GPS reflectivity data is utilized for weather forecast [14, 172]. GPS consists of 28 satellites which orbit approximately at an altitude of 12427 miles. Two different methods are discussed below:

2.4.10.1 GPS Limb Sounding for Atmospheric Reflectivity

In GPS, the position of the receiver is determined by the signal travel time from the satellite to receiver [87]. GPS signal reaches at the receiver through multiple paths which are reflected from the surrounding objects and surfaces. These multipath signals can cause destructive or constructive interference depending on the location of the object. However, this reflection is being utilized to obtain useful information about the sea ice, ocean state, soil moisture, snow pack, and sea ice. The GPS transmitted EM signal wave length is approximately 0.2 m. The reflections from these environmental parameters are investigated and novel GPS limb sounding techniques have been developed which are also called the occultation method. This technique produces accurate profiles of reflectivity in atmosphere.

2.4.10.2 GPS for Precipitable Water

GPS signals are also used to monitor the amount of precipitable water which is the entire water vapor in the atmosphere between two points in a column [14]. Due to complex permittivity of the water vapor, it absorbs and delays the EM waves traveling through the atmosphere. This can be measured by using interferometric instrument and is mapped to water vapor content. Another device sun photometer is also used to measure precipitable water by measuring the collimated solar radiation and the columnar aerosol optical depth (AOD).

2.5 Climate IoT Monitoring Systems

2.5.1 Cloud Properties Monitoring

The sensing of the vertical and horizontal distribution of macroscopic properties of clouds is done using active and passive remote sensing equipment [46, 145, 161]. The ceilometer is used to produce the vertical backscatter profile for cloud base height measurements. The Cloud, Aerosol Polarization and Backscatter LiDAR (CAPABL) is another type of cloud properties measurement tool. The microphysical cloud properties (e.g., shapes, sizes, water, and ice phases of the cloud particles) are also determined.

Microphysical Properties of Clouds The cloud properties sensing also involves microphysical measurements of thorough physical dimensions of the hydrometeor (an atmospheric phenomena related to clouds that involves water, water vapor, rain and other time varying characteristics of the clouds) [27, 29, 56, 88]. These measured hydrometeor characteristics are related to its phase, water and ice content, size, optics, and radar recurring properties.

Macrophysical Properties of Clouds The macrophysical properties of clouds involve measurements of cloud level parameters of clouds, that includes their place and position, dimensions, location, type, and the path of water and ice [28, 84, 85].

The cloud profiling instrument (profiler) operates in three different wavelengths. These include 915 MHz ultra-high frequency band, 2.835 GHz microwave band, and 50 MHz very high frequency. The radar sends energy and receives the back-scattered waves. Two types of turbulence phenomena are observed in these bands: Bragg scattering from reflectivity and Rayleigh scattering from hard objects. In these spectrum bands, the moisture and temperature are the primary sources of Bragg scattering, whereas the organic objects and hydrometers are the main cause of Rayleigh scattering. These instruments are used to observe atmospheric hydrometers.

2.5.2 Atmospheric Emissions Monitoring

The emission's scenarios [108] including different radiatively actives substances such as greenhouse gases and aerosols are monitored using LiDARs and other equipment which measures optical and scattering properties, size distribution, and aerosols extinction. This includes atmospheric monitoring for vertical and horizontal moisture, thermal, and kinetic properties and concentration of CO_2 and O_3 gases (e.g., radiatively active traces) using air-borne and surface based instruments.

2.5.3 Monitoring of the Surface of the Earth

The monitoring of the surface of the Earth involves measurements taken on, alongside, and underneath (less than two meters in the subsurface) the earth's earth-air interface. These observations ascertain characteristics such as soil's temperature and soil's volumetric water content, reflectivity of earth surface, momentum flux, latent and sensible heat, moisture, and CO_2 [34, 72, 100]. The numerical weather prediction models use these observations of earth surface, above ground and underground temperature, soil moisture, temperature of the radiative Earth skin, and surface reflectivity to provide current and foretasted values of these phenomena.

Surface Meteorology The land-based observations close to the Earth-air interface including precipitation, air temperature and pressure, moist content, and wind speed and direction are done using surface meteorology [70, 73].

Upper Air State Another important element of earth monitoring is the upper air state. The measurement techniques include balloon-borne, areal, and satellite-based observations. Many important parameters of the atmospheric profiles include geo-potential height, wind, moisture, temperature, and air pressure to support weather prediction models by providing input of these vital parameters.

2.5.4 Sea State Monitoring

The accurate information about the sea state is vital for weather forecasting and marine traffic [17]. The knowledge of sea state along with heat and moisture fluxes at multiple provide useful information at multiple scales. The sea state monitoring is the one using radars and drones. Other important sea state monitoring parameters include status of Arctic changes such as sea ice melting process, decline in sea-ice extent and thickness, wind and ocean circulation in North Atlantic. These are discussed in the next section.

2.5.4.1 OceanSITES

The OceanSITES is a network of global measurement stations for ocean to sea-floor and air-sea interaction monitoring [140]. It measures the surface and water column automated using sensors. The observations made using OceanSITES includes water transport, ocean acidification, meteorology, bio-geo-chemistry, carbon cycle, physical oceanography, and geophysics.

2.5.4.2 Air-Sea Heat Fluxes

In Atlantic observing system, the transport mooring arrays (TMAs) are employed in Atlantic Ocean to acquire long-term data of heat, volume, and freshwater fluxes of significantly strong flows. The air-sea heat-flux calculation is important for wave dynamics, kinematic and thermodynamic sensitivity analysis [171].

2.5.5 Arctic Measurements

The increasing temperatures have caused the rapid warming of the Arctic at a large scale due to which its sea cover has reduced. It has also induced the variation in heat

reflection and absorption from the ocean. The sunlight scattering, transmission, and absorption mechanisms of ice, snow, and water are different. Arctic measurements will play a vital role to get insights into the changing global weather patterns [24, 31, 53, 57, 85, 86, 115, 125, 148, 152, 156, 161, 169].

2.5.6 Hurricane Monitoring

To predict hurricane path and its intensity [103], reliable weather models are necessary. However, many physical model components that play a critical hurricanes are not understood very well and more measurements needed. In this regard, the identification and parameterization of heat fluxes and momentum over sea-air interface are required. The extension of similar analysis to the spray-filled transition layer is also needed for better accurate path prediction. The climate IoT with it capabilities of atmospheric observations and empirical measurement sin lab settings, coupled with models these parameterizations of sea-air momentum, and the heat flux can be better understood hurricane conditions. Different hurricane models are:

- The Global Forecast System (GFS)
- United Kingdom Meteorology (UKMET)
- Hurricane Weather Forecast Model (HWRF)
- Geophysical Fluid Dynamics Laboratory (GFDL)
- The European Medium Range Forecast Model (ECMWF)
- Navy Operational Global Prediction System (NOGAPS)

2.5.7 Solar Radiation Monitoring

Solar Radiation Network (SolRad-Net) is a network of sensors to provide high frequency solar flux measurements [135]. The Aerosol Robotic Network (AERONET) is network of distributed dynamic sun photometers to enable different ocean related applications [50]. The aerosol optical depth is done using the maritime aerosol network (MAN) element of AERONET. These measurements can be used to validate satellite, ground, and other aerosol based measurements.

A list of field testbeds with functionality and sensing capabilities for climate IoT integration is shown in Table 2.1.

2.6 Climate Databases Integration to IoT and Cloud

Climate IoT is envisioned as paradigm to manage and leverage the data from sensors and monitoring systems. Through cloud integration, it can handle complex data sets of high volume to support decision support systems designed to address complex

Table 2.1 A list of field testbeds with functionality and sensing capabilities for climate IoT integration

Testbed	Description
Arctic clouds in summer experiment	Observation of ice and sea conditions, clouds, atmospheric composition, and energy budget of earth surface
Boulder atmospheric observatory	Boundary layer analysis and long-term climate baseline measurements using is a 300 m meteorological tower for instruments
California nexus	Air quality and climate change airborne measurements using aircraft and surface measurements using mobile platform as well as fixed ground stations
CalWater	Analysis of atmospheric rivers and aerosols in clouds and precipitation using areal, ground, and sea-based measurements
Colorado airborne multi-phase study	Clouds and precipitation investigations
Coordinated observations of the lower arctic atmosphere	Low atmosphere thermodynamics analysis
Denver-Julesburg basin air quality study	Analysis of hydro-carbon emissions from gas and oil to observe methane
Dynamics of the Madden–Julian oscillation	Flux, sonde, and W-band radar measurements for MJO analysis
Front range air pollution and photochemistry testbed	Wind profilers/RASS and surface meteorology sensors for photochemistry, oxidant and aerosol formation and fate, flow and recirculation patterns
Discover air quality testbed	Air quality and pollution measurements
High wind gas exchange	Air-sea flux and wave observations
NOAA hydrometeorology testbed	High-impact regional precipitation, weather and land surface conditions analysis
Hurricane and severe storm sentinel	Hurricane formation and intensity change analysis in the Atlantic ocean basin
Intl arctic systems for observing the atmosphere	Arctic atmospheric observations of air-sea-ice flux, boundary layer dynamics, and clouds
Integrated characterization of energy, clouds, atmospheric state, and precipitation at summit	The clouds and precipitation analysis over the Greenland ice sheet using radar, LiDAR, precipitation, and radiosonde
Midlatitude continental convective clouds testbed	Cloud and precipitation analysis using radars
RV Mirai Arctic	Surface fluxes measurements using sonic anemometers and radiometers
Sea state	Wave and energy fluxes analysis during ice expansion at boundary layer

(continued)

Table 2.1 (continued)

Testbed	Description
Sensing hazards with operational unmanned technology	High impact weather prediction using unmanned observations
Storm peak cloud properties validation	Mixed-phase clouds and precipitation analysis using aircraft
Swedish–Russian–U.S. Arctic testbed	Cloud and boundary-layer observations with remote sensing equipment
Tropical ocean tropospheric exchange	Air-sea flux measurements of carbon monoxide
Uinta basin winter ozone	Tower-based measurements of surface fluxes, and ground-based measurements of surface, net irradiance, and meteorological variables
Wind forecast improvement testbed	Wind forecasting and wind energy modeling and applications
Hawaii ocean timeseries testbed	The climate observations using flux reference buoy sites
Winter storms and Pacific atmospheric rivers	Dropsonde system operations and data analysis to observe winter storms and Pacific atmospheric rivers
Experimental PBL instrumentation assessment	Remote sensing instrumentation for wind energy
Advanced vertical atmospheric profiling system	Global hawk dropsonde unmanned aircraft for atmospheric observations

environmental problems. Climate IoT also provides the opportunity design novel tools for searching, sharing, analysis, and visualization of data. A list of such data sets is given in Table 2.2.

2.7 IoT Enabled Indices

The climate IoT enables integration of following vital indices:

2.7.1 Air Quality Index (AQI)

AQI is an air quality pollution index [102]. The AQI index is determined for various air pollutants including sulfur dioxide, particle pollution, ground level ozone, and carbon monoxide. For each of these pollutants, the AirNow is used to report current and future pollution forecasts.

Table 2.2 Climate databases

Name	Data set description	Technology used in collection
International surface pressure data bank	The world's largest collection of pressure observations from 1856 to 2012. The ISPDv3 is a blend of many national and international collections of station, marine, and tropical cyclone best track pressure observations	Miscellaneous
Arctic summer cloud ocean cloud database	Cloud macro and microphysical measurements	Ka-band cloud radar, multichannel radiometer, and ceilometer
Arctic summer cloud ocean wind profiler database	Wind profiles and backscatter	449 MHz wind profiler radar
Daily hydro-meteorological data set for Mexico, the conterminous U.S., and southern Canada: 1950–2013	Hydrologic states, precipitation, maximum and minimum daily temperature and fluxes	A 6 km gridded product station
Hydrologic rainfall analysis XMRG data set	Four years of the California Nevada River Forecast Center (CNRFC) precipitation and temperature data sets with the XMRG	Miscellaneous
Air-sea flux	Ship-based flux observations	Satellite observations
Global ensemble forecast system reforecast data set	A 150 TB data set of global ensemble forecasts and a wide range of experimental forecast guidance based on these, including week-2 temperature and precipitation forecasts, week +1 precipitation forecasts, weeks +1 to +2 tornado forecasts	Miscellaneous
Worldview	More than 800 global, full-resolution satellite imagery layers for ash plumes, air quality, dust, drought, fires, severe storms, floods, smoke, water and ice, settlements, vegetation, and temperature	Satellite
Web soil survey (WSS)	Source of comprehensive soil related information	In-situ soil moisture measurements
Wave exposure model (WEMo)	Wind wave energy and the movement of seafloor sediment in enclosed water bodies such as lakes, coastal bays, and estuaries	Miscellaneous
Multiscale integrated models of ecosystem services (MIMES)	Georeferenced data sets as well as knowledge of ecological, economic, and social processes	Miscellaneous

2.7.2 Drought Index (EDDI)

The Evaporative Demand Drought Index (EDDI) [109] is drought monitoring and early warning tool. It provides early warning of developing drought and status of current droughts. The Standardized Precipitation Index (SPI) is another drought index used to monitor meteorological droughts.

2.7.3 Environmental Sensitivity Index (ESI)

The information about the coastal resources and other hazards such as oil spill, and sensitive shorelines can be obtained from ESI [52]. The ESI maps are utilized for hazard planning, to set safety priorities and practices.

2.7.4 Coastal Drought Index Using Salinity Data

Based on salinity data, a coastal salinity index (CSI) has been developed which provides monthly precipitation along with monthly mean salinity data to ascertain the probability of salinity for a specific month [129].

2.7.5 Wildfire Threat Index (SAWTI)

SAWTI is an index to forecast the fire potential by considering the wind potential. Surface temperature and relative humidity are the vital parameters for these fire-prone wind events monitoring [134].

2.8 Environmental Sensing Systems

In this section, different atmospheric sensing systems are discussed. A detailed list of these systems is given in Table 2.3.

2.8.1 Precipitation Occurrence Sensor System

The precipitation occurrence sensor system (POSS) is a type of Doppler radar that operates in X-band for precipitation sensing. It can sense type, intensity, and

Table 2.3 Environmental monitoring systems

Tool	Description
Twentieth century reanalysis	Global reconstruction of weather every 6 h from the surface of the earth to the tropopause back to 1851
Automated frost/heat forecast system	Frost and heat occurrences prediction in Vineyards
Atmos. river water vapor flux tool	Combines observations of wind profiles and integrated water vapor (IWV) to measure the IWV flux in the controlling layer and compares to operational numerical weather prediction prior and future forecasts
Atmospheric river detection tool	Automated objective software package to aid in the identification and characterization of atmospheric rivers to assist forecasters
Fairall–Banner sea-spray flux algorithm	A set of computer codes that allow estimation of air-sea momentum, heat, and moisture fluxes at hurricane wind speeds. Accounts for the effects of sea spray
Forecast reference evapotranspiration (FRET)	Bias-correction of FRET
Hydrologic model performance assessment tool	Set of R codes for calculating the performance metrics of hydrologic modeling. The developed metrics include Nash–Sutcliffe efficiency, runoff volume difference, modified correlation coefficient, percent bias, and time to peak. These functions can also automatically detect the miss of the USGS streamflow data to ensure the model assessment being executed on the apple-to- apple basis
Integrated characterization of energy, clouds, atmospheric state, and precipitation	Web page hosting near-real time measurements and data products from a suite of ground-based remote and in situ sensors characterizing the atmosphere, clouds, and precipitation at summit station on top of the Greenland ice sheet
MRMS NetCDF-XMRG format transformation tool	A set of Python codes which can transform the 1-km resolution multi-radar multi-sensor (MRMS) QPEs between the NetCDF and XMRG format. The tool also possesses the capabilities to perform the geo-reference and aggregation functions.
NOAA COARE bulk flux algorithm	A set of computer codes that allow estimation of air-sea or air-ice fluxes using bulk meteorological inputs. Meteorological and numerous trace gas fluxes are available
Snow-level product	A patented method to detect the level of the atmosphere where snow changes into rain

(continued)

Table 2.3 (continued)

Tool	Description
Vertical profile tool	Website allows users to extract different atmospheric products showing the vertical profile of the atmosphere. The products include single or multiple profiles on a date, a vertical transect between 2 points, a skew-T plot and a time by height plot. Data is extracted from different reanalyses and starts in 1871.
Vertically integrated water vapor transport (IVT) GIS tool	A python-based function which can automatically calculate water vapor transport at each pressure level and take integral of them. The domain covers the Pacific Ocean, Western US, and Southern Alaska. The tool is suitable for calculating IVTs for the variables extracted from the MERRA and NARR data sets.
WRIT: web-based reanalysis intercomparison tools	A set of web tools for plotting maps and time series that allows users to compare reanalysis and observed data sets.
Climate registry for the assessment of vulnerability	Assessments of the vulnerability of various natural and human resources to a changing climate
Climate resilience toolkit	Enable decision-makers to take action to boost their climate resilience using data-driven tools, information, and subject-matter expertise to make smarter decisions
Planning framework for a climate-resilient economy	Help communities recognize their economic vulnerabilities
Smart growth fixes for climate adaptation and resilience	Codes and policies for climate change

occurrence of precipitation and provides measurements of liquid precipitation and solid precipitation [122].

2.8.2 Radiosonde Temperature and Humidity Sensing

A radiosonde contains atmospheric sensing instrument (e.g., radiometers) installed on a weather balloon to measures different atmospheric parameters and transmission to ground stations. These are generally launched in open seas and ocean for temperature and humidity measurements and provides resolution of up to 10 km depending on the balloon flight altitude and capabilities of sensing instrument [21].

2.8.3 Cloud, Aerosol Polarization and Backscatter LiDAR (CAPABL)

The CAPBL is a tool to measure depolarization, particle orientation, and the backscatter of clouds and aerosols [145].

2.8.4 Operational Bright-Band Snow Level Sensing

A Doppler-effect based atmospheric profiling radar is employed to sense bright band snow levels (the heights in atmosphere at which snow becomes rain) from the atmospheric reflectivity and vertical Doppler velocity [162]. Another type, FM-CW snow level radar, uses advanced low transmit power frequency modulation of continuous waveform technique, which only uses less than a watt of transmitted power. It operates in 2835 MHz frequency band which is useful for precipitation properties measurements due to very weak attenuation/absorption of radio waves by moisture in this frequency spectrum.

2.8.5 Atmosphere Tomography Using Acoustic

In acoustic, travel time of sound waves is measured using array of horizontally located (up to 100 m high) acoustic tomography transmitters and receivers for temperature and wind velocity analysis [168].

2.8.6 Automated Atmospheric River Detection

Atmospheric river (AR) consists of narrow quills of high water vapor transport that leads to flooding [89, 105, 113, 132, 165, 166]. The identification and characterization of atmospheric river events are done using satellite and CALJET aircraft observations in the areas of integrated water vapor and transport (IWV and IVI) [130, 131, 141, 165]. It is based on integrated water vapor thresholds (e.g., width, length, core IWV contents of different features). A comparison of different detection criterion is given in [165]. A list of environmental monitoring systems is given in Table 2.3.

2.9 Case Studies

2.9.1 Indian Ocean Tsunami Warning System

In Indian Ocean tsunami warning system water and wave flow is measured using the whereby kinetic sensors [60]. These sensors are deployed in the ocean bed. These sensors can transmit data from the ocean floor which can be received by disk buoys afloat. The tsunami warnings are issued using these warning systems. The sensors communicate to buoys using acoustic technology for sea floor to surface communications and then use satellite links to warning systems.

2.9.2 Undersea Cables as Seismic Sensors

In an ITU project, sensors are deployed submarine cables to detect earthquakes and seismic events. Moreover, the fiber optic cables, on the ocean floor can also be used as seismic sensors can predict tsunamis, and provide insights into global seismic activity without any disruption to the service [54].

2.9.3 Connected Alarm Systems for Fast Moving Fires

Due to close proximity of home fires can spread quickly in urban slums. A red cross project in high density urban slums is using low cost, low energy, solar power sensors sense and alert authorities about the emerging fast moving fires, its location, and threat. It is deployed in Nairobi and Cape Town [153].

2.9.4 Urban Air Quality Sensing

Air quality sensors are employed to sense air in fresh air in Benin urban areas to track quantity and variations of pollutants. These sensors can sense and sense data with duty cycling period of 20 min using 3G wireless technology [5].

2.9.5 Water Flow Sensors

To monitor hydrological data about river levels and flows, water flow sensors are being used in developing countries. These sonar range water stream sensors can determine the distance to water surface [1].

References

1. Abegaz, B. W., Datta, T., & Mahajan, S. M. (2018). Sensor technologies for the energy-water nexus–a review. *Applied Energy, 210*, 451–466.
2. Abramowitz, G., Herger, N., Gutmann, E., Hammerling, D., Knutti, R., Leduc, M., et al. (2019). ESD reviews: Model dependence in multi-model climate ensembles: Weighting, sub-selection and out-of-sample testing. *Earth System Dynamics, 10*(1), 91–105.
3. Acquistapace, C., Kneifel, S., Löhnert, U., Kollias, P., Maahn, M., & Bauer-Pfundstein, M. (2017). Optimizing observations of drizzle onset with millimeter-wavelength radars. *Atmospheric Measurement Techniques, 10*(5), 1783–1802.
4. Adams, R. M., Hurd, B. H., Lenhart, S., & Leary, N. (1998). Effects of global climate change on agriculture: an interpretative review. *Climate Research, 11*(1), 19–30.
5. Ahuja, K., & Jani, N. (2019). Air quality prediction data-model formulation for urban areas. In *International Conference on Computer Networks and Communication Technologies* (pp. 111–118). Berlin: Springer.
6. Albergel, C., Munier, S., Bocher, A., Bonan, B., Zheng, Y., Draper, C., et al. (2018). LDAS-monde sequential assimilation of satellite derived observations applied to the contiguous us: An era-5 driven reanalysis of the land surface variables. *Remote Sensing, 10*(10), 1627.
7. Alexander, L., Zhang, X., Peterson, T., Caesar, J., Gleason, B., Klein Tank, A., et al. (2006). Global observed changes in daily climate extremes of temperature and precipitation. *Journal of Geophysical Research: Atmospheres, 111*(D5), 1–22.
8. Alexander, M. A., Kilbourne, K. H., & Nye, J. A. (2014). Climate variability during warm and cold phases of the Atlantic multidecadal oscillation (AMO) 1871–2008. *Journal of Marine Systems, 133*, 14–26.
9. Alexander, M. A., Scott, J. D., Friedland, K. D., Mills, K. E., Nye, J. A., Pershing, et al. (2018). Projected sea surface temperatures over the 21st century: Changes in the mean, variability and extremes for large marine ecosystem regions of northern oceans. *Elementa Science of the Anthropocene 6*(1), 1–25.
10. Bagley, J. E., Jeong, S., Cui, X., Newman, S., Zhang, J., Priest, C., et al. (2017). Assessment of an atmospheric transport model for annual inverse estimates of California greenhouse gas emissions. *Journal of Geophysical Research Atmospheres, 122*(3), 1901–1918.
11. Banta, R. M., Pichugina, Y. L., Brewer, W. A., James, E. P., Olson, J. B., Benjamin, S. G., et al. (2018). Evaluating and improving NWP forecast models for the future: How the needs of offshore wind energy can point the way. *Bulletin of the American Meteorological Society, 99*(6), 1155–1176.
12. Barsugli, J., Anderson, C., Smith, J. B., & Vogel, J. M. (2009). Options for improving climate modeling to assist water utility planning for climate change. Water Utility Climate Alliance White Paper. http://www.wucaonline.org/assets/pdf/pubs_whitepaper_120909.pdf
13. Bell, M. L., Goldberg, R., Hogrefe, C., Kinney, P. L., Knowlton, K., Lynn, B., et al. (2007). Climate change, ambient ozone, and health in 50 US cities. *Climatic Change, 82*(1–2), 61–76.
14. Bevis, M., Businger, S., Chiswell, S., Herring, T. A., Anthes, R. A., Rocken, C., et al. (1994). GPS meteorology: Mapping zenith wet delays onto precipitable water. *Journal of Applied Meteorology, 33*(3), 379–386.
15. Bianco, L., Friedrich, K., Wilczak, J. M., Hazen, D., Wolfe, D., Delgado, R., et al. (2017). Assessing the accuracy of microwave radiometers and radio acoustic sounding systems for wind energy applications. *Atmospheric Measurement Techniques, 10*(5), 1707.
16. Booker, F., Muntifering, R., McGrath, M., Burkey, K., Decoteau, D., Fiscus, E., et al. (2009). The ozone component of global change: Potential effects on agricultural and horticultural plant yield, product quality and interactions with invasive species. *Journal of Integrative Plant Biology, 51*(4), 337–351.

17. Bourassa, M. A., Gille, S. T., Jackson, D. L., Roberts, J. B., & Wick, G. A. (2010). Ocean winds and turbulent air-sea fluxes inferred from remote sensing. *Oceanography, 23*(4), 36–51.
18. Castro, S., Emery, W., Wick, G., & Tandy, W. (2017). Submesoscale sea surface temperature variability from UAV and satellite measurements. *Remote Sensing, 9*(11), 1089.
19. Castro, S. L., Monzon, L. A., Wick, G. A., Lewis, R. D., & Beylkin, G. (2018). Subpixel variability and quality assessment of satellite sea surface temperature data using a novel high resolution multistage spectral interpolation (HRMSI) technique. *Remote Sensing of Environment, 217*, 292–308.
20. Chisolm, E. I., & Matthews, J. C. (2012). Impact of hurricanes and flooding on buried infrastructure. *Leadership and Management in Engineering, 12*(3), 151–156.
21. Choi, B. I., Lee, S. W., Woo, S. B., Kim, J. C., Kim, Y. G., & Yang, S. G. (2018). Evaluation of radiosonde humidity sensors at low temperature using ultralow-temperature humidity chamber. *Advances in Science and Research, 15*, 207–212.
22. Choukulkar, A., Brewer, W. A., Sandberg, S. P., Weickmann, A., Bonin, T. A., Hardesty, R. M., et al. (2017). Evaluation of single and multiple Doppler lidar techniques to measure complex flow during the XPIA field campaign. *Atmospheric Measurement Techniques, 10*(1), 247–264.
23. Collins, III, C., Blomquist, B., Persson, O., Lund, B., Rogers, W., Thomson, J., et al. (2017). Doppler correction of wave frequency spectra measured by underway vessels. *Journal of Atmospheric and Oceanic Technology, 34*(2), 429–436.
24. Creamean, J. M., Kirpes, R. M., Pratt, K. A., Spada, N. J., Maahn, M., Boer, G. D., et al. (2018). Marine and terrestrial influences on ice nucleating particles during continuous springtime measurements in an arctic oilfield location. *Atmospheric Chemistry and Physics, 18*(24), 18023–18042.
25. Cynthia, R., David, R., Andrew, L.: *Our warming planet: Topics in climate dynamics* (vol. 1). Singapore: World Scientific.
26. Shupe, M. D. (2017). SOnic Detection And Ranging (SODAR) measurements taken at Summit Station, Greenland, 2017. http://doi.org/10.18739/A2V698B7K.
27. Shupe, M. D. (2018). Ceilometer Cloud Base Height Measurements at Summit Station, Greenland, 2018. Arctic Data Center. http://doi.org/10.18739/A2KP7TQ9P.
28. Shupe, M. D. (2018). Millimeter Cloud Radar measurements taken at Summit Station, Greenland, 2018. Arctic Data Center. http://doi.org/10.18739/A2F47GT18.
29. Shupe, M. D. (2018). Cloud and Aerosol Polarization and Backscatter LiDAR measurements taken at Summit Station, Greenland, 2018. Arctic Data Center. http://doi.org/10.18739/A25T3FZ9D.
30. Darwin, R., Tsigas, M. E., Lewandrowski, J., & Raneses, A. (1995). World agriculture and climate change: Economic adaptations. Tech. rep.
31. de Boer, G., Ivey, M., Schmid, B., Lawrence, D., Dexheimer, D., Mei, F., et al. (2018). A bird's-eye view: Development of an operational ARM unmanned aerial capability for atmospheric research in Arctic Alaska. *Bulletin of the American Meteorological Society, 99*(6), 1197–1212.
32. Diez, J. M., D'Antonio, C. M., Dukes, J. S., Grosholz, E. D., Olden, J. D., Sorte, C. J., et al. (2012). Will extreme climatic events facilitate biological invasions? *Frontiers in Ecology and the Environment, 10*(5), 249–257.
33. Doney, S. C., Fabry, V. J., Feely, R. A., & Kleypas, J. A. (2009). Ocean acidification: The other co2 problem. *Annual Review of Marine Science, 1*, 169–192.
34. Dorigo, W., de Jeu, R., Chung, D., Parinussa, R., Liu, Y., Wagner, W., et al. (2012). Evaluating global trends (1988–2010) in harmonized multi-satellite surface soil moisture. *Geophysical Research Letters, 39*(18), 1–7.
35. Draper, C., & Reichle, R. H. (2019). Assimilation of satellite soil moisture for improved atmospheric reanalyses. *Monthly Weather Review, 147*(6), 2163–2188.

36. Du, Y., Song, W., He, Q., Huang, D., Liotta, A., & Su, C. (2019). Deep learning with multi-scale feature fusion in remote sensing for automatic oceanic eddy detection. *Information Fusion, 49*, 89–99.
37. Duarte-Guardia, S., Peri, P. L., Amelung, W., Sheil, D., Laffan, S. W., Borchard, N., et al. (2019). Better estimates of soil carbon from geographical data: A revised global approach. *Mitigation and Adaptation Strategies for Global Change, 24*(3), 355–372.
38. Easterling, W. E. (2011). *Guidelines for adapting agriculture to climate change*. London: Imperial College Press.
39. Emery, W., Castro, S., Wick, G., Schluessel, P., & Donlon, C. (2001). Estimating sea surface temperature from infrared satellite and in situ temperature data. *Bulletin of the American Meteorological Society, 82*(12), 2773–2786.
40. Fairall, C. W., Bradley, E. F., Rogers, D. P., Edson, J. B., & Young, G. S. (1996). Bulk parameterization of air-sea fluxes for tropical ocean-global atmosphere coupled-ocean atmosphere response experiment. *Journal of Geophysical Research Oceans, 101*(C2), 3747–3764.
41. Fairall, C., Matrosov, S. Y., Williams, C. R., & Walsh, E. (2018). Estimation of rain rate from airborne Doppler w-band radar in calwater-2. *Journal of Atmospheric and Oceanic Technology, 35*(3), 593–608.
42. Fan, Y., Miguez-Macho, G., Weaver, C. P., Walko, R., & Robock, A. (2007). Incorporating water table dynamics in climate modeling: 1. water table observations and equilibrium water table simulations. *Journal of Geophysical Research: Atmospheres, 112*(D10), 1–17.
43. FEMA. (2013). Mitigation assessment team report: Hurricane sandy in New Jersey and New York.
44. Fowler, D. R., Mitchell, C. S., Brown, A., Pollock, T., Bratka, L. A., Paulson, J., et al. (2013). Heat-related deaths after an extreme heat event-four states, 2012, and united states, 1999–2009. *MMWR Morbidity and Mortality Weekly Report, 62*(22), 433.
45. Friel, S., Dangour, A. D., Garnett, T., Lock, K., Chalabi, Z., Roberts, I., et al. (2009). Public health benefits of strategies to reduce greenhouse-gas emissions: Food and agriculture. *The Lancet, 374*(9706), 2016–2025.
46. Fu, S., Deng, X., Shupe, M. D., & Xue, H. (2019). A modelling study of the continuous ice formation in an autumnal arctic mixed-phase cloud case. *Atmospheric Research, 228*, 77–85.
47. Gan, T. Y., Barry, R. G., Gizaw, M., Gobena, A., & Balaji, R. (2013). Changes in North American snowpacks for 1979–2007 detected from the snow water equivalent data of SMMR and SSM/I passive microwave and related climatic factors. *Journal of Geophysical Research: Atmospheres, 118*(14), 7682–7697.
48. Gao, Y., Vano, J. A., Zhu, C., & Lettenmaier, D. P. (2011). Evaluating climate change over the Colorado River basin using regional climate models. *Journal of Geophysical Research Atmospheres, 116*(D13), 1–20.
49. Gao, Y., Leung, L. R., Salathé, Jr, E. P., Dominguez, F., Nijssen, B., & Lettenmaier, D. P. (2012). Moisture flux convergence in regional and global climate models: Implications for droughts in the Southwestern United States under climate change. *Geophysical Research Letters, 39*(9), 1–5.
50. García, O., Díaz, A., Expósito, F., Díaz, J., Dubovik, O., Dubuisson, P., et al. (2008). Validation of AERONET estimates of atmospheric solar fluxes and aerosol radiative forcing by ground-based broadband measurements. *Journal of Geophysical Research Atmospheres, 113*(D21).
51. Gastineau, G., Soden, B. J., Jackson, D. L., & O'dell, C. W. (2014). Satellite-based reconstruction of the tropical oceanic clear-sky outgoing longwave radiation and comparison with climate models. *Journal of Climate, 27*(2), 941–957.
52. Gil-Agudelo, D. L., Ibarra-Mojica, D. M., Guevara-Vargas, A. M., Nieto-Bernal, R., Serrano-Gómez, M., Gundlach, E. R., et al. (2019). Environmental sensitivity index for oil spills in Colombian rivers (ESI-R): Application for the Magdalena river. *CT&F-Ciencia, Tecnología y Futuro, 9*(1), 83–91.

53. Grachev, A. A., Persson, P. O. G., Uttal, T., Akish, E. A., Cox, C. J., Morris, S. M., et al. (2018). Seasonal and latitudinal variations of surface fluxes at two arctic terrestrial sites. *Climate Dynamics, 51*(5–6), 1793–1818.
54. Grall, G., & Moresco, G. (2002). System for undersea seismic prospecting. US Patent 6,456,565.
55. Greene, S., Kalkstein, L. S., Mills, D. M., & Samenow, J. (2011). An examination of climate change on extreme heat events and climate–mortality relationships in large us cities. *Weather, Climate, and Society, 3*(4), 281–292.
56. Greenwald, T. J., Stephens, G. L., Vonder Haar, T. H., & Jackson, D. L. (1993). A physical retrieval of cloud liquid water over the global oceans using special sensor microwave/imager (SSM/I) observations. *Journal of Geophysical Research Atmospheres, 98*(D10), 18471–18488.
57. Guest, P., Persson, P. O. G., Wang, S., Jordan, M., Jin, Y., Blomquist, B., et al. (2018). Low-level baroclinic jets over the new Arctic ocean. *Journal of Geophysical Research Oceans, 123*(6), 4074–4091.
58. Haines, A., McMichael, A. J., Smith, K. R., Roberts, I., Woodcock, J., Markandya, A., et al. (2009). Public health benefits of strategies to reduce greenhouse-gas emissions: Overview and implications for policy makers. *The Lancet, 374*(9707), 2104–2114.
59. Hamill, T. M., Engle, E., Myrick, D., Peroutka, M., Finan, C., & Scheuerer, M. (2017). The US national blend of models for statistical postprocessing of probability of precipitation and deterministic precipitation amount. *Monthly Weather Review, 145*(9), 3441–3463.
60. Hanka, W., Saul, J., Weber, B., Becker, J., Harjadi, P., Rudloff, A., et al. (2010). Real-time earthquake monitoring for tsunami warning in the Indian ocean and beyond. *Natural Hazards & Earth System Sciences, 10*(12), 2611–2622.
61. Hartten, L. M., Johnston, P. E., Rodríguez Castro, V. M., & Esteban Pérez, P. S. (2019). Postdeployment calibration of a tropical UHF profiling radar via surface-and satellite-based methods. *Journal of Atmospheric and Oceanic Technology, 36*, 1729–1751. https://doi.org/10.1175/JTECH-D-18-0020.1.
62. Hatfield, J. L., Boote, K. J., Kimball, B. A., Ziska, L., Izaurralde, R.C., Ort, D., et al. (2011). Climate impacts on agriculture: Implications for crop production. *Agronomy Journal, 103*(2), 351–370.
63. Heimlich, B., & Bloetscher, F. (2011). Effects of sea level rise and other climate change impacts on southeast Florida's water resources. *Florida Water Resources Journal, 63*(9), 37–48.
64. Herron, T., Tolstoy, I., & Kraft, D. (1969). Atmospheric pressure background fluctuations in the mesoscale range. *Journal of Geophysical Research, 74*(6), 1321–1329.
65. Hodgkins, G. A., & Dudley, R. W. (2006). Changes in late-winter snowpack depth, water equivalent, and density in Maine, 1926–2004. *Hydrological Processes an International Journal, 20*(4), 741–751.
66. Högström, U., & Smedman, A. S. (2004). Accuracy of sonic anemometers: Laminar wind-tunnel calibrations compared to atmospheric in situ calibrations against a reference instrument. *Boundary-Layer Meteorology, 111*(1), 33–54.
67. Huang, D., Zhang, Q., Wang, J., Liotta, A., Song, W., & Zhu, J. (2018). Marine information system based on ocean data ontology construction. In *2018 IEEE International Conference on Systems, Man, and Cybernetics (SMC)* (pp. 2595–2601). Piscataway: IEEE.
68. Izaurralde, R. C., Thomson, A. M., Morgan, J., Fay, P., Polley, H., & Hatfield, J. L. (2011). Climate impacts on agriculture: Implications for forage and rangeland production. *Agronomy Journal, 103*(2), 371–381.
69. Jackson, D. L., & Stephens, G. L. (1995). A study of SSM/I-derived columnar water vapor over the global oceans. *Journal of Climate, 8*(8), 2025–2038.
70. Jackson, D. L., & Wick, G. A. (2010). Near-surface air temperature retrieval derived from AMSU-A and sea surface temperature observations. *Journal of Atmospheric and Oceanic Technology, 27*(10), 1769–1776.

71. Jackson, D. L., & Wick, G. A. (2014). Propagation of uncertainty analysis of co2 transfer velocities derived from the COARE gas transfer model using satellite inputs. *Journal of Geophysical Research Oceans, 119*(3), 1828–1842.
72. Jackson, D. L., Wick, G. A., & Bates, J. J. (2006). Near-surface retrieval of air temperature and specific humidity using multisensor microwave satellite observations. *Journal of Geophysical Research Atmospheres, 111*(D10), 1–16.
73. Jackson, D. L., Wick, G. A., & Robertson, F. R. (2009). Improved multisensor approach to satellite-retrieved near-surface specific humidity observations. *Journal of Geophysical Research Atmospheres, 114*(D16), 1–13.
74. Jagtap, S., Jones, J., Mearns, L., Ojima, D., Paul, E., & Paustian, K. (2003). US agriculture and climate change: New results. *Climatic Change, 57*, 4369.
75. Jeong, S., Newman, S., Zhang, J., Andrews, A. E., Bianco, L., Dlugokencky, E., et al. (2018). Inverse estimation of an annual cycle of California's nitrous oxide emissions. *Journal of Geophysical Research Atmospheres, 123*(9), 4758–4771.
76. Jin, X., Yu, L., Jackson, D. L., & Wick, G. A. (2015). An improved near-surface specific humidity and air temperature climatology for the SSM/I satellite period. *Journal of Atmospheric and Oceanic Technology, 32*(3), 412–433.
77. Johnson, D. L., Ambrose, S. H., Bassett, T. J., Bowen, M. L., Crummey, D. E., Isaacson, J. S., et al. (1997). Meanings of environmental terms. *Journal of Environmental Quality, 26*(3), 581–589.
78. Joseph, A. (2014). Chapter 4 - remote mapping of sea surface currents using HF Doppler radar networks. In A. Joseph (Ed.), *Measuring ocean currents* (pp. 109–137). Boston: Elsevier. https://doi.org/10.1016/B978-0-12-415990-7.00004-1.
79. Justić, D., Rabalais, N. N., & Turner, R. E. (2005). Coupling between climate variability and coastal eutrophication: Evidence and outlook for the Northern Gulf of Mexico. *Journal of Sea Research, 54*(1), 25–35.
80. Karl, T. R., Melillo, J. M., Peterson, T. C., & Hassol, S. J. (2009). *Global climate change impacts in the United States*. Cambridge: Cambridge University Press.
81. Khan, R., Khan, S. U., Zaheer, R., & Khan, S. (2012). Future internet: The internet of things architecture, possible applications and key challenges. In *2012 10th International Conference on Frontiers of Information Technology* (pp. 257–260). IEEE (2012)
82. Kundzewicz, Z. W., Budhakooncharoen, S., Bronstert, A., Hoff, H., Lettenmaier, D., Menzel, L., et al. (2002). Coping with variability and change: Floods and droughts. In *Natural resources forum* (vol. 26, pp. 263–274). Wiley Online Library.
83. Kunkel, K. (2008). Observed changes in weather and climate extremes. In *Weather and climate extremes in a changing climate: Regions of focus: North America, Hawaii, Caribbean, and US Pacific Islands* (pp. 35–80). Scotts Valley: CreateSpace Independent.
84. Lacour, A., Chepfer, H., Shupe, M. D., Miller, N. B., Noel, V., Kay, J., et al. (2017). Greenland clouds observed in CALIPSO-GOCCP: Comparison with ground-based summit observations. *Journal of Climate, 30*(15), 6065–6083.
85. Liu, Y., Shupe, M. D., Wang, Z., & Mace, G. (2017). Cloud vertical distribution from combined surface and space radar-lidar observations at two arctic atmospheric observatories. *Atmospheric Chemistry and Physics, 17*(9), 5973–5989.
86. Lund, B., Graber, H. C., Persson, P., Smith, M., Doble, M., Thomson, J., et al. (2018). Arctic sea ice drift measured by shipboard marine radar. *Journal of Geophysical Research: Oceans, 123*(6), 4298–4321.
87. Ma, Z., Kuo, Y. H., Ralph, F. M., Neiman, P. J., Wick, G. A., Sukovich, E., et al. (2018). Assimilation of GPS radio occultation data for an intense atmospheric river with the NCEP regional GSI system. *Monthly Weather Review, 139*(7), 2170–2183.
88. Maahn, M., Hoffmann, F., Shupe, M. D., Boer, G. D., Matrosov, S. Y., & Luke, E. P. (2019). Can liquid cloud microphysical processes be used for vertically pointing cloud radar calibration? *Atmospheric Measurement Techniques, 12*(6), 3151–3171.

89. Mahoney, K., Jackson, D. L., Neiman, P., Hughes, M., Darby, L., Wick, G., et al. (2016). Understanding the role of atmospheric rivers in heavy precipitation in the southeast united states. *Monthly Weather Review, 144*(4), 1617–1632.
90. Maizlish, N., Woodcock, J., Co, S., Ostro, B., Fanai, A., & Fairley, D. (2013). Health cobenefits and transportation-related reductions in greenhouse gas emissions in the San Francisco bay area. *American Journal of Public Health, 103*(4), 703–709.
91. Malaver Rojas, J. A., Motta, N., Gonzalez, L. F., Corke, P., & Depari, A. (2012). Towards the development of a gas sensor system for monitoring pollutant gases in the low troposphere using small unmanned aerial vehicles. In R. N. Smith (Ed.), *Workshop on Robotics for Environmental Monitoring, 11 July 2012, Sydney University, N. S. W*.
92. Markandya, A., Armstrong, B. G., Hales, S., Chiabai, A., Criqui, P., Mima, S., et al. (2009). Public health benefits of strategies to reduce greenhouse-gas emissions: Low-carbon electricity generation. *The Lancet, 374*(9706), 2006–2015.
93. Marlier, M. E., DeFries, R. S., Voulgarakis, A., Kinney, P. L., Randerson, J. T., Shindell, D. T., et al. (2013). El niño and health risks from landscape fire emissions in Southeast Asia. *Nature Climate Change, 3*(2), 131.
94. Mass, C., Skalenakis, A., & Warner, M. (2011). Extreme precipitation over the west coast of North America: Is there a trend? *Journal of Hydrometeorology, 12*(2), 310–318.
95. Matrosov, S. Y. (2017). Characteristic raindrop size retrievals from measurements of differences in vertical Doppler velocities at Ka-and W-band radar frequencies. *Journal of Atmospheric and Oceanic Technology, 34*(1), 65–71.
96. Matrosov, S. Y., & Turner, D. D. (2018). Retrieving mean temperature of atmospheric liquid water layers using microwave radiometer measurements. *Journal of Atmospheric and Oceanic Technology, 35*(5), 1091–1102.
97. McCaffrey, K., Bianco, L., Johnston, P., & Wilczak, J. M. (2017). A comparison of vertical velocity variance measurements from wind profiling radars and sonic anemometers. *Atmospheric Measurement Techniques, 10*(3), 999.
98. McCaffrey, K., Bianco, L., & Wilczak, J. M. (2017). Improved observations of turbulence dissipation rates from wind profiling radars. *Atmospheric Measurement Techniques, 10*(7), 2595–2611.
99. McCaffrey, K., Quelet, P. T., Choukulkar, A., Wilczak, J. M., Wolfe, D. E., Oncley, S. P., et al. (2017). Identification of tower-wake distortions using sonic anemometer and lidar measurements. *Atmospheric Measurement Techniques, 10*(NREL/JA-5000-68031), 393–407.
100. McVicar, T. R., Roderick, M. L., Donohue, R. J., Li, L. T., Van Niel, T. G., Thomas, A., et al. (2012). Global review and synthesis of trends in observed terrestrial near-surface wind speeds: Implications for evaporation. *Journal of Hydrology, 416*, 182–205.
101. Mir, L. (2008). Indoor residential chemical emissions as risk factors for respiratory and allergic effects in children: A review. *Environnement, Risques & Santé, 7*(1), 10–11.
102. Mirabelli, M., Sarnat, S., & Damon, S. (2019). Air quality index and air quality awareness among adults in the united states. In *C45. Effects of the environment on pulmonary health*, pp. A4909–A4909. New York: American Thoracic Society.
103. Mohanty, U., & Gupta, A. (2008). Deterministic methods for prediction of tropical cyclone tracks. In *Modelling and monitoring of coastal marine processes* (pp. 141–170). Berlin: Springer.
104. Mueller, J. L., Bidigare, R., Trees, C., Balch, W., Dore, J., Drapeau, D., et al. (2003). *Ocean optics protocols for satellite ocean color sensor validation, revision 5. Volume v: Biogeochemical and bio-optical measurements and data analysis protocols*. Greenbelt: Goddard Space Flight Space Center.
105. Mueller, M. J., Mahoney, K. M., & Hughes, M. (2017). High-resolution model-based investigation of moisture transport into the Pacific Northwest during a strong atmospheric river event. *Monthly Weather Review, 145*(9), 3861–3879.
106. Murphy, M. (1994). Weathering the storm: Water systems versus hurricanes. *Journal-American Water Works Association, 86*(1), 74–83.

107. Myers, D. R. (2016). *Solar radiation: Practical modeling for renewable energy applications*. Boca Raton: CRC Press.
108. Nakicenovic, N., Alcamo, J., Grubler, A., Riahi, K., Roehrl, R., Rogner, H. H., et al. (2000). *Special report on emissions scenarios (SRES), a special report of Working Group III of the intergovernmental panel on climate change*. Cambridge: Cambridge University Press.
109. Nam, W. H., Feng, S., Hayes, M. J., Svoboda, M. D., Fuchs, B., Hong, E. M., et al. (2018). Flash drought risk assessment over China and Korea using evaporative demand drought index (EDDI). In *AGU fall meeting abstracts*.
110. National Research Council, Division on Earth and Life Studies, Board on Atmospheric Sciences and Climate, Committee on Stabilization Targets for Atmospheric Greenhouse Gas Concentrations. (2011). *Climate stabilization targets: Emissions, concentrations, and impacts over decades to millennia*. Washington: National Academies Press.
111. Neiman, P. J., Ralph, F. M., White, A., Kingsmill, D., & Persson, P. (2002). The statistical relationship between upslope flow and rainfall in California's coastal mountains: Observations during CALJET. *Monthly Weather Review, 130*(6), 1468–1492.
112. Neiman, P. J., Wick, G. A., Ralph, F. M., Martner, B. E., White, A.B., & Kingsmill, D. E. (2005). Wintertime nonbrightband rain in California and Oregon during CALJET and PACJET: Geographic, interannual, and synoptic variability. *Monthly Weather Review, 133*(5), 1199–1223.
113. Neiman, P. J., Gaggini, N., Fairall, C. W., Aikins, J., Spackman, J. R., Leung, L.R., et al. (2017). An analysis of coordinated observations from NOAA's Ronald H. Brown ship and G-IV aircraft in a landfalling atmospheric river over the North Pacific during CalWater-2015. *Monthly Weather Review, 145*(9), 3647–3669.
114. Newsom, R. K., Brewer, W. A., Wilczak, J. M., Wolfe, D., Oncley, S., & Lundquist, J. K. (2017). Validating precision estimates in horizontal wind measurements from a Doppler lidar. *Atmospheric Measurement Techniques, 10*(3), 1229–1240.
115. Norgren, M. S., Boer, G. D., & Shupe, M. D. (2018). Observed aerosol suppression of cloud ice in low-level arctic mixed-phase clouds. *Atmospheric Chemistry and Physics, 18*(18), 13345–13361.
116. Parris, A. S., Bromirski, P., Burkett, V., Cayan, D. R., Culver, M. E., Hall, J., et al. (2012). Global sea level rise scenarios for the united states national climate assessment. NOAA technical report OAR CPO.
117. Patz, J. A., McGeehin, M. A., Bernard, S. M., Ebi, K. L., Epstein, P. R., Grambsch, A., et al. (2000). The potential health impacts of climate variability and change for the united states: Executive summary of the report of the health sector of the us national assessment. *Environmental Health Perspectives, 108*(4), 367–376.
118. Perlwitz, J., & Graf, H. F. (1995). The statistical connection between tropospheric and stratospheric circulation of the Northern Hemisphere in winter. *Journal of Climate, 8*(10), 2281–2295.
119. Perlwitz, J., Knutson, T., Kossin, J. P., & LeGrande, A. N. (2017). Large-scale circulation and climate variability. In D. J. Wuebbles, D. W. Fahey, K. A. Hibbard, D. J. Dokken, B. C. Stewart, & T. K. Maycock (Eds.) *Climate Science special report: Fourth national climate assessment*. U.S. Global Change Research Program (Vol. I, pp. 161–184). http://doi.org/10.7930/J0RV0KVQ.
120. Peterson, T. C., Stott, P. A., & Herring, S. (2012). Explaining extreme events of 2011 from a climate perspective. *Bulletin of the American Meteorological Society, 93*(7), 1041–1067.
121. Peterson, T. C., Heim, Jr., R. R., Hirsch, R., Kaiser, D. P., Brooks, H., Diffenbaugh, N. S., et al. (2013). Monitoring and understanding changes in heat waves, cold waves, floods, and droughts in the united states: State of knowledge. *Bulletin of the American Meteorological Society, 94*(6), 821–834.
122. Pettersen, C., Bennartz, R., Merrelli, A. J., Shupe, M. D., Turner, D. D., & Walden, V. P. (2018). Precipitation regimes over central Greenland inferred from 5 years of ICECAPS observations. *Atmospheric Chemistry and Physics, 18*(7), 4715–4735.

123. Pichugina, Y. L., Banta, R. M., Olson, J. B., Carley, J. R., Marquis, M. C., Brewer, W. A., et al. (2017). Assessment of NWP forecast models in simulating offshore winds through the lower boundary layer by measurements from a ship-based scanning Doppler lidar. *Monthly Weather Review, 145*(10), 4277–4301.
124. Polvani, L. M., Sun, L., Butler, A. H., Richter, J.H., & Deser, C. (2017). Distinguishing stratospheric sudden warmings from ENSO as key drivers of wintertime climate variability over the north Atlantic and Eurasia. *Journal of Climate, 30*(6), 1959–1969.
125. Popovicheva, O., Diapouli, E., Makshtas, A., Shonija, N., Manousakas, M., Saraga, D., et al. (2019). East Siberian Arctic background and black carbon polluted aerosols at HMO Tiksi. *Science of the Total Environment, 655*, 924–938.
126. Potyrailo, R. A. (2016). Multivariable sensors for ubiquitous monitoring of gases in the era of internet of things and industrial internet. *Chemical Reviews, 116*(19), 11877–11923.
127. Privette, J., Fowler, C., Wick, G., Baldwin, D., & Emery, W. (1995). Effects of orbital drift on advanced very high resolution radiometer products: Normalized difference vegetation index and sea surface temperature. *Remote Sensing of Environment, 53*(3), 164–171.
128. Pruski, F. F., & Nearing, M. A. (2002). Runoff and soil-loss responses to changes in precipitation: A computer simulation study. *Journal of Soil and Water Conservation, 57*(1), 7–16.
129. Rahman, M. M., Mostofa, M. G., Rahman, M. A., Miah, M. G., Saha, S. R., Karim, M. A., et al. (2019). Insight into salt tolerance mechanisms of the halophyte Achras sapota: An important fruit tree for agriculture in coastal areas. *Protoplasma, 256*(1), 181–191.
130. Ralph, F. M., Neiman, P. J., & Wick, G. A. (2004). Satellite and CALJET aircraft observations of atmospheric rivers over the eastern north Pacific ocean during the winter of 1997/98. *Monthly Weather Review, 132*(7), 1721–1745.
131. Ralph, F., Iacobellis, S., Neiman, P., Cordeira, J., Spackman, J., Waliser, D., et al. (2017). Dropsonde observations of total integrated water vapor transport within North Pacific atmospheric rivers. *Journal of Hydrometeorology, 18*(9), 2577–2596.
132. Ralph, F. M., Dettinger, M., Lavers, D., Gorodetskaya, I. V., Martin, A., Viale, M., et al. (2017). Atmospheric rivers emerge as a global science and applications focus. *Bulletin of the American Meteorological Society, 98*(9), 1969–1973.
133. Roberts, J., Clayson, C., Robertson, F., & Jackson, D. (2010). Predicting near-surface characteristics from SSM/I using neural networks with a first guess approach. *Journal of Geophysical Research, 115*, D19113.
134. Rolinski, T., Capps, S. B., & Zhuang, W. (2019). Santa Ana winds: A descriptive climatology. *Weather and Forecasting, 34*(2), 257–275.
135. Rosário, N. E., Yamasoe, M. A., Brindley, H., Eck, T. F., & Schafer, J. (2011). Downwelling solar irradiance in the biomass burning region of the southern Amazon: Dependence on aerosol intensive optical properties and role of water vapor. *Journal of Geophysical Research Atmospheres, 116*(D18), 1–10.
136. Sanchez-Cohen, I., Díaz-Padilla, G., Velasquez-Valle, M., Slack, D. C., Heilman, P., & Pedroza-Sandoval, A. (2015). A decision support system for rainfed agricultural areas of Mexico. *Computers and Electronics in Agriculture, 114*, 178–188.
137. Sands, R. D., & Edmonds, J. A. (2005). Climate change impacts for the conterminous USA: An integrated assessment. In: *Climate change impacts for the conterminous USA* (pp. 127–150). Berlin: Springer.
138. Schaller, M. F., & Fan, Y. (2009). River basins as groundwater exporters and importers: Implications for water cycle and climate modeling. *Journal of Geophysical Research Atmospheres, 114*(D4), 1–21.
139. Scheuerer, M., & Hamill, T. M. (2018). Generating calibrated ensembles of physically realistic, high-resolution precipitation forecast fields based on GEFS model output. *Journal of Hydrometeorology, 19*(10), 1651–1670.

140. Send, U., Wallace, D. W. R., Lampitt, R., Honda, M. C., Lukas, R., Feely R., et al. (2009). OceanSITES. In *Proceedings of OceanObs'09: Sustained Ocean Observations and Information for Society*. Paris: European Space Agency. http://dx.doi.org/10.5270/OceanObs09.cwp.79.
141. Shields, C. A., Rutz, J. J., Leung, L. Y., Ralph, F. M., Wehner, M., Kawzenuk, B., et al. (2018). Atmospheric river tracking method intercomparison project (ARTMIP): Project goals and experimental design. *Geoscientific Model Development, 11*(6), 2455–2474.
142. Smit, B., & Skinner, M. W. (2002). Adaptation options in agriculture to climate change: A typology. *Mitigation and Adaptation Strategies for Global Change, 7*(1), 85–114.
143. Sossa, A., Liebmann, B., Bladé, I., Allured, D., Hendon, H.H., Peterson, P., et al. (2017). Statistical connection between the Madden–Julian oscillation and large daily precipitation events in west Africa. *Journal of Climate, 30*(6), 1999–2010.
144. Spickett, J. T., Brown, H., & Rumchev, K. (2011). Climate change and air quality: The potential impact on health. *Asia Pacific Journal of Public Health, 23*(2), 37S–45S.
145. Stillwell, R. A., Neely, III, R. R., Thayer, J. P., Shupe, M. D., & Turner, D. D. (2018). Improved cloud-phase determination of low-level liquid and mixed-phase clouds by enhanced polarimetric lidar. *Atmospheric Measurement Techniques, 11*(2), 835–859.
146. Stone, B., Hess, J. J., & Frumkin, H. (2010). Urban form and extreme heat events: Are sprawling cities more vulnerable to climate change than compact cities? *Environmental Health Perspectives, 118*(10), 1425–1428.
147. Strauch, R. G., Merritt, D., Moran, K., Earnshaw, K., & De Kamp, D. V. (1984). The Colorado wind-profiling network. *Journal of Atmospheric and Oceanic Technology, 1*(1), 37–49.
148. Sun, L., Alexander, M., & Deser, C. (2018). Evolution of the global coupled climate response to Arctic sea ice loss during 1990–2090 and its contribution to climate change. *Journal of Climate, 31*(19), 7823–7843.
149. Tagaris, E., Manomaiphiboon, K., Liao, K. J., Leung, L. R., Woo, J. H., He, S., et al. (2007). Impacts of global climate change and emissions on regional ozone and fine particulate matter concentrations over the united states. *Journal of Geophysical Research Atmospheres, 112*(D14), 1–11.
150. Tao, F., Zuo, Y., Da Xu, L., Lv, L., & Zhang, L. (2014). Internet of things and BOM-based life cycle assessment of energy-saving and emission-reduction of products. *IEEE Transactions on Industrial Informatics, 10*(2), 1252–1261.
151. Trenberth, K. E. (2011). Changes in precipitation with climate change. *Climate Research, 47*(1–2), 123–138.
152. Turner, D., Shupe, M., & Zwink, A. (2018). Characteristic atmospheric radiative heating rate profiles in arctic clouds as observed at barrow, Alaska. *Journal of Applied Meteorology and Climatology, 57*(4), 953–968.
153. Twigg, J., Christie, N., Haworth, J., Osuteye, E., & Skarlatidou, A. (2017). Improved methods for fire risk assessment in low-income and informal settlements. *International Journal of Environmental Research and Public Health, 14*(2), 139.
154. United States Environmental Protection Agency. (2013). *Inventory of us greenhouse gas emissions and sinks: 1990–2011* (vol. 505). Washington DC: United States Environmental Protection Agency.
155. Vose, R. S., Applequist, S., Bourassa, M. A., Pryor, S. C., Barthelmie, R. J., Blanton, B., et al. (2014). Monitoring and understanding changes in extremes: Extratropical storms, winds, and waves. *Bulletin of the American Meteorological Society, 95*(3), 377–386.
156. Walden, V., & Shupe, M. (2013). Radiosonde temperature and humidity profiles taken at summit station, Greenland, Arctic Data Center.
157. Wall, E., & Smit, B. (2005). Climate change adaptation in light of sustainable agriculture. *Journal of Sustainable Agriculture, 27*(1), 113–123.
158. Walthall, C. L., Hatfield, J., Backlund, P., Lengnick, L., Marshall, E., Walsh, M., et al. (2012). Climate change and agriculture in the United States: Effects and adaptation (p. 186). Washington: USDA Technical Bulletin 1935.

159. Wang, Y., Li, J., & Wang, H. H. (2019). Cluster and cloud computing framework for scientific metrology in flow control. *Cluster Computing, 22*(1), 1189–1198.
160. Wen, Y., Behrangi, A., Chen, H., & Lambrigtsen, B. (2018). How well were the early 2017 California atmospheric river precipitation events captured by satellite products and ground-based radars? *Quarterly Journal of the Royal Meteorological Society, 144*, 344–359.
161. Wendisch, M., Macke, A., Ehrlich, A., Lüpkes, C., Mech, M., Chechin, D., et al. (2019). The Arctic cloud puzzle: Using ACLOUD/PASCAL multiplatform observations to unravel the role of clouds and aerosol particles in arctic amplification. *Bulletin of the American Meteorological Society, 100*(5), 841–871.
162. White, A. B., Gottas, D. J., Ralph, F. M., & Neiman, P. J. (2003). Operational bright-band snow level detection using Doppler radar. US Patent 6,615,140.
163. Wick, G. A., Bates, J. J., & Gottschall, C. C. (2000). Observational evidence of a wind direction signal in SSM/I passive microwave data. *IEEE transactions on Geoscience and Remote Sensing, 38*(2), 823–837.
164. Wick, G. A., Bates, J. J., & Scott, D. J. (2002). Satellite and skin-layer effects on the accuracy of sea surface temperature measurements from the goes satellites. *Journal of Atmospheric and Oceanic Technology, 19*(11), 1834–1848.
165. Wick, G. A., Neiman, P. J., & Ralph, F. M. (2012). Description and validation of an automated objective technique for identification and characterization of the integrated water vapor signature of atmospheric rivers. *IEEE Transactions on Geoscience and Remote Sensing, 51*(4), 2166–2176.
166. Wick, G. A., Neiman, P. J., Ralph, F. M., & Hamill, T. M. (2013). Evaluation of forecasts of the water vapor signature of atmospheric rivers in operational numerical weather prediction models. *Weather and Forecasting, 28*(6), 1337–1352.
167. Wilkinson, P., Smith, K. R., Davies, M., Adair, H., Armstrong, B. G., Barrett, M., et al. (2009). Public health benefits of strategies to reduce greenhouse-gas emissions: Household energy. *The Lancet, 374*(9705), 1917–1929.
168. Wilson, D., Ziemann, A., Ostashev, V., & Voronovich, A. (2001). An overview of acoustic travel-time tomography in the atmosphere and its potential applications. *Acta Acustica United with Acustica, 87*(6), 721–730.
169. Wood, K. R., Jayne, S. R., Mordy, C. W., Bond, N., Overland, J. E., Ladd, C., et al. (2018). Results of the first arctic heat open science experiment. *Bulletin of the American Meteorological Society, 99*(3), 513–520.
170. Woodcock, J., Edwards, P., Tonne, C., Armstrong, B. G., Ashiru, O., Banister, et al. (2009). Public health benefits of strategies to reduce greenhouse-gas emissions: Urban land transport. *The Lancet, 374*(9705), 1930–1943.
171. Yu, L., & Weller, R. A. (2007). Objectively analyzed air–sea heat fluxes for the global ice-free oceans (1981–2005). *Bulletin of the American Meteorological Society, 88*(4), 527–540.
172. Zhang, J. A., Cione, J. J., Kalina, E. A., Uhlhorn, E. W., Hock, T., & Smith, J.A. (2017). Observations of infrared sea surface temperature and air–sea interaction in Hurricane Edouard (2014) using GPS dropsondes. *Journal of Atmospheric and Oceanic Technology, 34*(6), 1333–1349.
173. Ziska, L. H. (2011). Climate change, carbon dioxide and global crop production: Food security and uncertainty. *Handbook on Climate Change and Agriculture* (pp. 9–31). Cheltenham: Edward Elgar.
174. Salam A. (2020) Internet of Things for Sustainable Community Development: Introduction and Overview. In: Internet of Things for Sustainable Community Development. Internet of Things (Technology, Communications and Computing). Springer, Cham. DOI: https://doi.org/10.1007/978-3-030-35291-2_1
175. Salam A. (2020) Internet of Things for Environmental Sustainability and Climate Change. In: Internet of Things for Sustainable Community Development. Internet of Things (Technology, Communications and Computing). Springer, Cham. DOI: https://doi.org/10.1007/978-3-030-35291-2_2
176. Salam A. (2020) Internet of Things in Agricultural Innovation and Security. In: Internet of Things for Sustainable Community Development. Internet of Things (Technology, Communications and Computing). Springer, Cham. DOI: https://doi.org/10.1007/978-3-030-35291-2_3
177. Salam A. (2020) Internet of Things for Water Sustainability. In: Internet of Things for Sustainable Community Development. Internet of Things (Technology, Communications and Computing). Springer, Cham. DOI: https://doi.org/10.1007/978-3-030-35291-2_4

159. Salam A. (2020) Internet of Things for Sustainable Forestry. In: Internet of Things for Sustainable Community Development. Internet of Things (Technology, Communications and Computing). Springer, Cham. DOI: https://doi.org/10.1007/978-3-030-35291-2_5
160. Salam A. (2020) Internet of Things in Sustainable Energy Systems. In: Internet of Things for Sustainable Community Development. Internet of Things (Technology, Communications and Computing). Springer, Cham. DOI: https://doi.org/10.1007/978-3-030-35291-2_6
161. Salam A. (2020) Internet of Things for Sustainable Human Health. In: Internet of Things for Sustainable Community Development. Internet of Things (Technology, Communications and Computing). Springer, Cham. DOI: https://doi.org/10.1007/978-3-030-35291-2_7
162. Salam A. (2020) Internet of Things for Sustainable Mining. In: Internet of Things for Sustainable Community Development. Internet of Things (Technology, Communications and Computing). Springer, Cham. DOI: https://doi.org/10.1007/978-3-030-35291-2_8
163. Salam A. (2020) Internet of Things in Water Management and Treatment. In: Internet of Things for Sustainable Community Development. Internet of Things (Technology, Communications and Computing). Springer, Cham. 10.1007/978-3-030-35291-2_9
164. Salam A. (2020) Internet of Things for Sustainability: Perspectives in Privacy, Cybersecurity, and Future Trends. In: Internet of Things for Sustainable Community Development. Internet of Things (Technology, Communications and Computing). Springer, Cham. DOI: https://doi.org/10.1007/978-3-030-35291-2_10
165. Salam, A.; Hoang, A.D.; Meghna, A.; Martin, D.R.; Guzman, G.; Yoon, Y.H.; Carlson, J.; Kramer, J.; Yansi, K.; Kelly, M.; Skvarek, M.; Stankovic, M.; Le, N.D.K.; Wierzbicki, T.; Fan, X. The Future of Emerging IoT Paradigms: Architectures and Technologies. Preprints 2019, 2019120276 (doi: https://doi.org/10.20944/preprints201912.0276.v1).
166. A. Konda, A. Rau, M. A. Stoller, J. M. Taylor, A. Salam, G. A. Pribil, C. Argyropoulos, and S. A. Morin, "Soft microreactors for the deposition of conductive metallic traces on planar, embossed, and curved surfaces," Advanced Functional Materials, vol. 28, no. 40, p. 1803020. [Online]. Available: https://onlinelibrary.wiley.com/doi/abs/10.1002/adfm.201803020
167. A. Salam, M. C. Vuran, and S. Irmak, "Pulses in the sand: Impulse response analysis of wireless underground channel," in The 35th Annual IEEE International Conference on Computer Communications (INFOCOM 2016), San Fran- cisco, USA, Apr. 2016.
168. A. Salam and M. C. Vuran, "Impacts of soil type and moisture on the capacity of multi-carrier modulation in internet of underground things," in Proc. of the 25th ICCCN 2016, Waikoloa, Hawaii, USA, Aug 2016.
169. A. Salam, M. C. Vuran, and S. Irmak, "Towards internet of underground things in smart lighting: A statistical model of wireless underground channel," in Proc. 14th IEEE International Conference on Networking, Sensing and Control (IEEE ICNSC), Calabria, Italy, May 2017.
170. A. Salam and M. C. Vuran, "Smart underground antenna arrays: A soil moisture adaptive beamforming approach," in Proc. IEEE INFOCOM 2017, Atlanta, USA, May 2017.
171. ——, "Wireless underground channel diversity reception with multiple antennas for internet of underground things," in Proc. IEEE ICC 2017, Paris, France, May 2017.
172. ——, "EM-Based Wireless Underground Sensor Networks," in Underground Sensing, S. Pamukcu and L. Cheng, Eds. Academic Press, 2018, pp. 247 – 285.
173. A. Salam, M. C. Vuran, and S. Irmak, "Di-sense: In situ real- time permittivity estimation and soil moisture sensing using wireless underground communications," Computer Networks, vol. 151, pp. 31 – 41, 2019. [Online]. Available: http://www.sciencedirect.com/science/article/pii/ S1389128618303141
174. A. Salam and S. Shah, "Urban underground infrastructure monitoring IoT: the path loss analysis," in 2019 IEEE 5th World Forum on Internet of Things (WF- IoT) (WF-IoT 2019), Limerick, Ireland, Apr. 2019.
175. A. Salam, "Pulses in the sand: Long range and high data rate communication techniques for next generation wireless underground networks," ETD collection for University of Nebraska - Lincoln, no. AAI10826112, 2018. [Online]. Available: http://digitalcommons.unl.edu/dissertations/AAI10826112
176. A. Salam and S. Shah, "Internet of things in smart agriculture: Enabling technologies," in 2019 IEEE 5th World Forum on Internet of Things (WF-IoT) (WF-IoT 2019), Limerick, Ireland, Apr. 2019.
177. A. Salam, M. C. Vuran, X. Dong, C. Argyropoulos, and S. Irmak, "A theoretical model of underground dipole antennas for communications in internet of under- ground things," IEEE Transactions on Antennas and Propagation, 2019.

159. M. C. Vuran, A. Salam, R. Wong, and S. Irmak, “Internet of underground things: Sensing and communications on the field for precision agriculture,” in 2018 IEEE 4th World Forum on Internet of Things (WF-IoT) (WF-IoT 2018), Singapore, Feb. 2018.
160. ——, “Internet of underground things in precision agriculture: Architecture and technology aspects,” Ad Hoc Networks, 2018.
161. Salam A. (2020) Internet of Things for Sustainable Community Development. Springer, Cham. DOI: https://doi.org/10.1007/978-3-030-35291-2
162. A. Salam, “Underground soil sensing using subsurface radio wave propagation,” in 5th Global Workshop on Proximal Soil Sensing, COLUMBIA, MO, May 2019.
163. ——, “A comparison of path loss variations in soil using planar and dipole antennas,” in 2019 IEEE International Symposium on Antennas and Propagation. IEEE, Jul 2019.
164. ——, “A path loss model for through the soil wireless communications in digital agriculture,” in 2019 IEEE International Symposium on Antennas and Propagation. IEEE, Jul 2019.
165. ——, Underground Environment Aware MIMO Design Using Transmit and Receive Beamforming in Internet of Underground Things. Cham: Springer International Publishing, 2019, pp. 1–15.
166. A. Salam and U. Karabiyik, “A cooperative overlay approach at the physical layer of cognitive radio for digital agriculture,” in Third International Balkan Conference on Communications and Networking 2019 (BalkanCom’19), Skopje, Macedonia, the former Yugoslav Republic of, Jun. 2019.
167. A. Salam, “An underground radio wave propagation prediction model for digital agriculture,” Information, vol. 10, no. 4, 2019. [Online]. Available: http://www.mdpi.com/2078-2489/10/4/147
168. S. Temel, M. C. Vuran, M. M. Lunar, Z. Zhao, A. Salam, R. K. Faller, and C. Stolle, “Vehicle-to-barrier communication during real-world vehicle crash tests,” Computer Communications, vol. 127, pp. 172 – 186, 2018. [Online]. Available: http://www.sciencedirect.com/science/article/pii/ S0140366417305224
169. A. Salam, "Design of Subsurface Phased Array Antennas for Digital Agriculture Applications", in Proc. 2019 IEEE International Symposium on Phased Array Systems and Technology (IEEE Array 2019), Waltham, MA, USA, Oct 2019.
170. A. Salam, "Subsurface MIMO: A Beamforming Design in Internet of Underground Things for Digital Agriculture Applications", J. Sens. Actuator Netw., Volume 8, No. 3, August 2019. doi: 10.3390/jsan8030041